

Small System Collectivity in Relativistic Hadron and Nuclear Collisions

James L. Nagle¹ and William A. Zajc²

¹University of Colorado, Boulder, Colorado 80309, USA ; email:
jamie.nagle@colorado.edu

²Columbia University, NY, NY 10027, USA; email:waz1@columbia.edu

Ann. Rev. Nucl. Part. Sci. 2018. 68:1–33

This article's doi:
TBD

Copyright © 2018 by Annual Reviews.
All rights reserved

Keywords

QCD, RHIC, LHC, heavy-ion collisions, quark-gluon plasma,
relativistic hydrodynamics, perfect liquid

Abstract

The bulk motion of nuclear matter at the ultra-high temperatures created in heavy-ion collisions at the Relativistic Heavy Ion Collider and the Large Hadron Collider is well described in terms of nearly inviscid hydrodynamics, thereby establishing this system of quarks and gluons as the most perfect fluid in nature. A revolution in the field is underway, spearheaded by the discovery of similar collective, fluid-like phenomena in much smaller systems including $p + p$, $p + A$, $d + Au$, and $^3\text{He} + Au$ collisions. We review these exciting new observations and their implications.

Contents

1. Introduction	3
2. Historical Preludes	3
3. Standard Model of Heavy Ion Collisions	4
4. Small System Experimental Data	7
4.1. Two-particle Correlations and Initial Observations	8
4.2. Instructive Measurements	10
4.3. Limits of Small System Flow Behavior	13
5. Additional Considerations	14
5.1. Absence of Jet Quenching in Small Collision Systems	15
5.2. Initial Conditions	17
5.3. Parton Transport Models	18
5.4. Momentum Correlations Explanations	20
6. Hydrodynamic Discussion and Implications	21
7. Summary	24

1. Introduction

The modern era of heavy ion physics began in the year 2000 with first data-taking at the Relativistic Heavy Ion Collider (RHIC), followed by heavy ion running at the Large Hadron Collider (LHC) in 2010. Shortly thereafter, a new arena for studying high temperature nuclear matter came to the fore with a host of observations in small collision systems including $p + p$ and $p(d, {}^3\text{He})+A$ collisions. These smaller systems exhibited many of the features of collective behavior found in collisions of heavy nuclei attributed to the “perfect fluid” nature of quark-gluon plasma (QGP). While these observations were contrary to expectations, there is a long history of considering even small collision systems in the framework of hydrodynamics. This article begins with a brief review of that history, followed by an overview of observations from collisions of large nuclei (Au+Au and Pb+Pb) supporting the standard hydrodynamic model of heavy ion reactions. Next we highlight the most important observations in small collision systems that give evidence for similar underlying physics. We include a discussion of key additional considerations and alternative explanations. Finally we review the current status of the theoretical interpretation of these results.

2. Historical Preludes

Collective models of nuclear matter have a long history which is replete with controversy and in some cases rancor. Certainly Bohr’s compound nucleus (1) and the associated liquid-drop model (building on work of Gamow, Heisenberg and von Weizsäcker (2)) evoked little controversy, particularly after its quantitative success in explaining fission in ${}^{235}\text{U}$ (3). The underlying physical assumption of quasi-equilibration of energy was plausible when applied to reactions involving slow neutrons. Collective descriptions for higher energy collisions appeared to be less well-grounded. Heisenberg’s 1949 attempt (4) to understand excitations of the pion “fluid” was widely ignored. On the other hand, a year later Fermi’s statistical model (5) (which he acknowledged to be the extreme limit of Heisenberg’s approach) received considerable attention. Fermi argued that precisely because the interactions between pions and nucleons were strong, one could expect the available energy to be “rapidly . . . distributed among the various degrees of freedom according to statistical laws.” Taking the reaction volume as his only free parameter Fermi developed predictions (in modern terminology) for particle multiplicities in terms of n -body phase space, and presented a simple argument showing that in the high energy limit the number of produced particles N would vary with center-of-mass collision energy \sqrt{s} as $N \sim s^{1/4}$.

Fermi carefully qualified his statistical model’s “extreme” assumptions, noting that by working in the opposite regime from a perturbative approach, one might be able to bracket the correct theory. As noted by Herb Anderson in Fermi’s *Collected Papers* (6), “In the later literature this made it appear that this theory was always wrong; a point that Fermi didn’t enjoy at all.” A special case of such criticism was voiced by Landau (7), who after noting Fermi’s “ingenious idea”, goes on to write “the quantitative calculation given by him appears unconvincing to us and incorrect at several points.” In particular, Landau observes that the number of particles in the strongly interacting initial state is ill-defined (a point he attributes to Pomeranchuk (8)),

and that the distribution of final state particles may be calculated only at the endpoint of a *hydrodynamic* expansion. Landau also stated that the hydrodynamic motion would be that of "an ideal (non-viscous and non-heat-conducting) liquid." In subsequent work with Belenkij (9) Landau elaborated on this assertion, noting that the condition for the applicability of hydrodynamics $R \gg \ell_{mfp}$, where R is the least dimension of the system and ℓ_{mfp} is the mean free path, for a *relativistic* system necessarily leads to a large Reynolds number characteristic of inviscid systems. Expressing the Reynolds number in terms of the mass density ρ , the shear viscosity η , the "bulk" velocity V of the system and the microscopic velocity v of its constituents, one has

$$\mathcal{R}e \equiv \frac{\rho R V}{\eta} \sim \frac{\rho R V}{\rho \ell_{mfp} v} \sim \frac{R c}{\ell_{mfp} c} = \frac{R}{\ell_{mfp}} \gg 1 \quad . \quad (1)$$

Therefore, intrinsically relativistic systems in the hydrodynamic limit should have low (kinematic) viscosities.

Despite the pedigree of these early developments, it is fair to say that the hydrodynamic approach never entered the mainstream of hadronic physics in the second half of the 20th century. Rather, a variety of methods - phase shift analyses, S-matrix, bootstrap, etc. - were investigated before QCD emerged as the underlying field theory for the strong interaction in the 1970's. Not even the excellent hydrodynamic description of inclusive hadron rapidity distributions at FNAL fixed target energies and the CERN ISR (10) was able to gain traction against the subsequent enthusiasm for QCD's clear predictions for perturbative phenomena. One of the few exceptions to this general trend was Bjorken's simple and hugely influential model of hydrodynamic expansion in ultra-relativistic A+A collisions (11), which explicitly allowed for its application to p + p collisions.

Motivated by Bjorken's predictions, there were experimental searches for signatures of QGP formation in p + p and $\bar{p} + p$ collisions, including Tevatron experiments E735 (12)) and MiniMAX (13). No firm conclusions resulted from this program, in part due to the non-comprehensive nature of these experiments, for example MiniMAX exclusively searched for Disoriented Chiral Condensates (DCC). In hindsight, the DCC searches serve as an important reminder that when a region of disturbed vacuum eventually returns to the "normal" vacuum via particle emission the final number of hadrons may not be the relevant quantity to understand whether collectivity or hydrodynamics is applicable at earlier times. In the case of E735, baryon and strangeness modifications in high multiplicity events were a possible QGP signature, but also found explanations via autocorrelations between higher multiplicities and larger numbers of gluon jets. Recent measurements of strangeness enhancement of multi-strange baryons in p + p collisions at the LHC revive this important discussion (14). The field pushed forward to study the collisions of the largest nuclei at relativistic energies, first in the fixed target programs at the Brookhaven AGS and CERN SPS, and ultimately with the construction of RHIC and the LHC.

3. Standard Model of Heavy Ion Collisions

In 2001, early results from the RHIC program indicated that in head-on collisions of gold nuclei (Au+Au) at 200 GeV per nucleon pair, the majority of the energy is deposited into a medium

whose expansion is well described hydrodynamically, i.e. as a flowing fluid (15–18). The hydrodynamic nature of the matter was eventually quantified in terms of its shear viscosity, which turns out to be very close to the conjectured smallest possible ratio of viscosity to entropy density ($\frac{\eta}{s} \geq \frac{\hbar}{4\pi k_B} = \frac{1}{4\pi}$ in natural units) of any fluid (19, 20). This nuclear matter has a starting temperature of order 350-400 MeV, or equivalently four trillion Kelvin, and as such is composed of quarks and gluons no longer bound into color neutral hadrons such as protons and neutrons. Subsequent measurements of lead on lead (Pb+Pb) collisions at the LHC (21) at up to 5.02 TeV per nucleon pair display a similar fluidity with the matter starting at a higher initial temperature of order 400-600 MeV(22). In both cases, Au+Au and Pb+Pb collisions create a QGP that behaves as a nearly perfect fluid, i.e, one with $\frac{\eta}{s} \sim \frac{1}{4\pi}$.

Just as the Big Bang theory is the prevailing paradigm for the time evolution of the the early universe, over the last ten years the nuclear physics community has developed a Little Bang theory as the standard model for the time evolution of heavy ion collisions, a model described in detail in Refs. (23–27). The evolution can be broken into distinct epochs:

- (i) The highly Lorentz-contracted nuclei collide with a very short traversal time ($\ll 1$ fm/c). Predominantly through interactions of gluons in the nuclei, often described in terms of gluon fields, energy is deposited into the newly created medium. The initial, very inhomogeneous, distribution of deposited energy in the transverse plane, perpendicular to the beam direction, is referred to as the “initial condition.”
- (ii) The matter is initially out of equilibrium and some time is required for it to equilibrate. During this time the matter expands at nearly the speed of light in the longitudinal direction and begins to expand radially in the transverse plane. This is often referred to as the “pre-equilibrium” stage.
- (iii) After the matter is nearly equilibrated¹, it is modeled via viscous hydrodynamics using an equation of state from lattice QCD calculations. Deviations from equilibrium are accounted for with shear and bulk viscosity terms.
- (iv) The fluid cools to a temperature corresponding to the QGP crossover transition(31) $T \approx 170$ MeV (as determined by the inflection point of the Polyakov loop, roughly equivalent to the confinement-deconfinement transition) (32) and then breaks up into hadrons as most commonly modeled via Cooper-Frye freeze-out (33).
- (v) The resulting hadrons scatter, both inelastically until what is called chemical freeze-out

¹For most of a decade since the identification of the applicability of hydrodynamics to heavy ion collisions, the predominant thinking has been that for hydrodynamic calculations to be valid the system must be nearly equilibrated at an early time of order $\tau \approx 0.5 - 2.0$ fm/c. Thus the time before this point is referred to as pre-equilibrium, and an entire sub-area of the field has been devoted to the “rapid equilibration” puzzle, trying to answer the question of how does the system equilibrate so fast. However, recently it has been realized that the hot nuclear matter may never come close to equilibration (28–30) and that a different explanation justifies the applicability of hydrodynamics as we discuss in detail in Section 6. In this picture, the separation of stage (ii) and (iii) is really just “hydrodynamization” (the point where hydrodynamics is applicable) and the naming of stage (ii) as pre-equilibrium is misleading and should be simply “pre-hydrodynamization.”

and elastically until kinetic freeze-out, at which time they are assigned their final state momenta as measured experimentally.

Sophisticated computer modeling of large numbers of individual collisions follow each of these stages through to predictions for final hadrons that are measured in experiment. As with constraining properties of the early universe, this field has advanced to multi-parameter Bayesian analyses (34–38) to extract key properties of the medium, for example η/s , and to assess the correlated sensitivities of the extracted values to different assumptions for the initial conditions.

The matter produced in the collision is subjected to enormous longitudinal pressure, expanding at nearly the speed of light in this direction, often assumed to be boost invariant (11). There are also large pressure gradients in the transverse direction driven not only by the density differential to the vacuum outside the medium but also by inhomogeneities in the matter. Figure 1 (left panel) shows the temperature and flow profile of a A+A collision from a hydrodynamic model. A number of key features are worth detailing:

1. There is an overall pattern of strong radial outward expansion with the largest bulk velocities near the periphery reaching 75% of the speed of light.
2. At the end of the hydrodynamic epoch, one calculates the hadronization process in the rest frame of the fluid cell and then boosts hadrons into the lab frame. Thus, heavier hadrons receive a larger momentum shift (blue shift) which is measurable as a distinct feature in the transverse momentum (p_T) distribution of hadrons as a function of their mass.
3. The spatial distribution of the matter and its temperature profile are lumpy, despite the lumpiness of the initial condition already having been washed out to some degree by viscous effects. These inhomogeneities lead to substantial distortions in the azimuthal distribution of particles (39), which are quantified in terms of a Fourier expansion (40) as:

$$\frac{dn}{d\phi} \propto 1 + \sum_n 2v_n(p_T) \cos(n(\phi - \Psi_n)) \quad , \quad (2)$$

where p_T and ϕ are the transverse momentum and azimuthal angle of each particle and Ψ_n is the overall orientation of the n^{th} moment. The first four moments v_1 , v_2 , v_3 , and v_4 are often referred to as directed, elliptic, triangular, quadrangular flow coefficients, respectively.

4. Near mid-rapidity, for semi-central collisions, the dominant Fourier coefficient is v_2 , reflecting the efficient hydrodynamic translation via pressure gradients of the initial “almond-shaped” overlap region to momentum space. Again, because of the larger fluid velocities built up along directions of steeper pressure gradients, heavier hadrons will have their flow patterns $v_n(p_T)$ shifted outward in p_T as shown in Figure 1 (right panel).

Hydrodynamic calculations describe the measured higher-order coefficients v_3 to v_5 (41). Such comparisons constrain both the initial inhomogeneities that are the source of the fluid anisotropies, and the medium properties such as the shear viscosity that has a larger damping effect on the higher-order coefficients. There is a nice analogy between these v_n measurements in heavy ion physics reflecting the initial spatial anisotropies, and the spherical harmonic moment

measurements from the cosmic microwave background reflecting the earlier inhomogeneities in the early universe, giving key constraints on QGP properties from the former, and early universe properties from the latter.

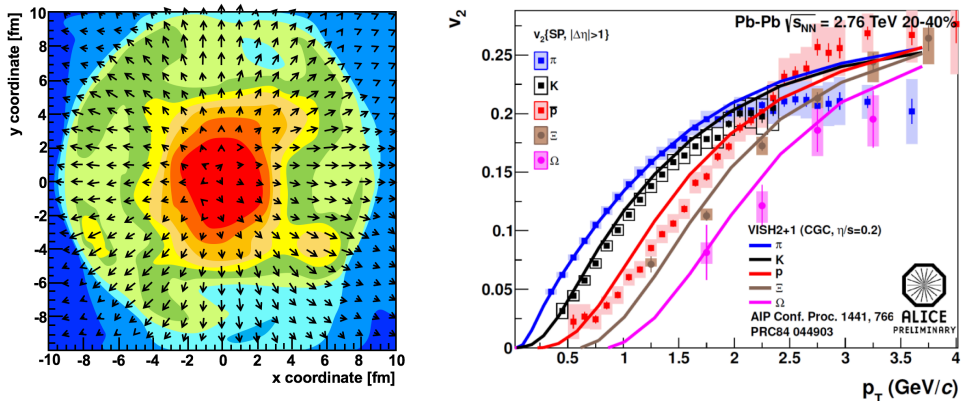


Figure 1

(Left) Viscous hydrodynamic calculation results of a semi-central A+A collision in one time snapshot ($t = 5$ fm/c). The color scale indicates the temperature of the fluid cells in the transverse (x - y) plane and the arrows represent the fluid velocity vectors with the lengths proportional to the speed. (Right) Elliptic flow coefficient $v_2(p_T)$ for identified hadrons in Pb+Pb collisions at the LHC, also compared with hydrodynamic calculations (42).

The standard model for A+A collisions is now well established and tested with great precision. This model describes a multitude of experimental measurements including the mass-dependent p_T spectra, the v_n flow coefficients, the distribution of event-by-event fluctuations in those flow coefficients, multi-particle correlations referred to as cumulants (43), and Hanbury-Brown Twiss (HBT) correlations (44). Other correlations between different flow coefficients that only arise from the non-linear mode mixing terms in hydrodynamics (45) are qualitatively described, leading Heinz and Snellings (24) to refer to this as an *experimentum crucis* in support of the hydrodynamic paradigm. There are some outstanding puzzles that may turn out to be reconciled within the standard framework (as was the case for the so-called HBT puzzle (46)), or be first hints of additional physics — specific examples include the flow moment ordering in ultra-central collisions (47) and thermal photon emission and anisotropy (48).

4. Small System Experimental Data

In the initial years of the heavy ion collider era, small colliding systems such as $p(d,^3\text{He})+A$ were regarded as control measurements. Measurements in $d+\text{Au}$ and $p+\text{Pb}$ at RHIC and the LHC

have been very useful, for example, in constraining nuclear modified parton distribution functions (nPDFs) that determine the initial gluon distributions that determine the first epoch of heavy ion collisions (49, 50). However, in 2010, the CMS experiment examined ultra-high multiplicity $p + p$ collisions at the LHC and found that particles had a weak, though clear, preference to be emitted along a common transverse ϕ angle across all rapidities (51). This sparked a scientific debate over whether this could be related to similar correlations observed in A+A, or was due to new physics coming from early-collision momentum correlations. Then in 2012, p +Pb data taking at the LHC, quickly followed by a re-examination of d +Au data at RHIC, revealed that most of the signatures for hydrodynamic flow in A+A also existed in these smaller systems. The revolution started by these small system measurements, and the attempt to reconcile them in the context of the above A+A standard model, is the focus of this review. We concentrate on those observables most directly related to collectivity while noting that there is a wealth of data not included on electroweak probes, strangeness enhancement, etc. and additional physics areas of interest regarding nuclear modified parton distribution functions, gluon saturation phenomena, multi-parton interactions, and color reconnection, among others.

4.1. Two-particle Correlations and Initial Observations

Crucial information regarding collectivity is garnered through the measurement of two or more particle correlations, often parameterized via the particles' relative azimuthal angle $\Delta\phi$ in the transverse plane, and their relative longitudinal pseudorapidity $\Delta\eta$. Since the reaction plane angles Ψ_n appearing in Equation 2 are assumed to reflect geometric features of the initial matter distribution common to all produced particles, standard Fourier properties lead to two-particle correlations proportional to $v_n^2 \cos(n\Delta\phi)$ that extend “long-range” in pseudorapidity as the matter expands longitudinally. Figure 2 shows two-particle correlations as a function of relative angles $\Delta\phi$ and $\Delta\eta$ as measured in $p + p$, p +Pb and Pb+Pb collisions at the LHC. In the Pb+Pb case, the long-range correlations dominate and were originally named the “ridge” around $\Delta\phi = 0$ and another “ridge” around $\Delta\phi = \pi$. In central collisions this second feature split into two “ridges” near $\Delta\phi \approx 2\pi/3, 4\pi/3$ and for a time were mistakenly interpreted as a “Mach cone” response from high energy quarks traversing the matter. These features are now understood in a fully unified picture (52) as arising from elliptic, triangular, and higher flow moments.

However, there are a number of sources for such correlations having nothing to do with a flowing medium. In a hydrodynamic description, all of these other correlation sources are referred to as “non-flow.” Simple examples include the decay of hadronic resonances, e.g. $\Delta^{++} \rightarrow p + \pi^+$, giving rise to a two-particle correlation. Large momentum-transfer scattering of partons from the incoming hadrons or nuclei can result in jets, i.e., two collimated sprays of hadrons that are nearly back-to-back in azimuth ($\Delta\phi \approx \pi$) and with a correlation in pseudorapidity depending on the momentum fractions x_1, x_2 of the incoming partons. Even low momentum-transfer scattering of initial partons can result in “long-range” correlations as a consequence of total momentum conservation. These contributions are evident in correlation measurements in all collision systems from e^+e^- , $p + p$, and A+A to varying degrees and must be accounted for in order to isolate the

contribution from flow physics.

In the Pb+Pb case, in addition to the dominant flow contributions, there is a localized peak near $\Delta\phi \approx \Delta\eta \approx 0$ due to correlations amongst a small number of particles from single jet fragmentation, resonance decay, etc. Because hadrons from a single fragmenting jet are in a cone, they are easily distinguished from the “long-range” flow contribution around $\Delta\phi = 0$. However, the dijet partner, while approximately back-to-back in azimuth can swing in pseudorapidity, resulting in a “long-range” correlation around $\Delta\phi = \pi$, which is more challenging to disentangle from flow. In the A+A case, these dijet correlations are sub-dominant for $p_T < 5$ GeV/c. Also shown in Figure 2 are the same two-particle correlations in p +Pb and $p + p$ collisions at the LHC. One observes the near-side “ridge” in both cases, though with weaker strength, and a larger away-side “ridge”, from the combination of flow correlations and non-flow contributions. These features represent the first evidence for flow-like collective behavior in a small system:

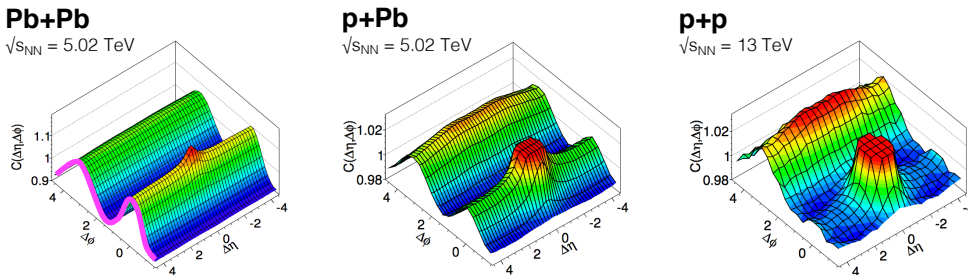


Figure 2

Shown are two-particle correlation results in Pb+Pb (left), p +Pb (middle), and $p + p$ (right) collisions at the LHC (53). As highlighted by the magenta curve, in Pb+Pb collisions there is a large $\cos(2\Delta\phi)$ correlation with peaks at $\Delta\phi = 0, \pi$ that extend long-range in pseudorapidity $\Delta\eta$. A similar feature is observed in p +Pb and $p + p$ collisions, though not dominating the overall correlations to the same degree.

high multiplicity $p + p$ collisions at the LHC exhibit a long-range near-side “ridge” in azimuthal correlations, very similar to that observed in A+A collisions. Because of the unexpected nature of the “ridge” as a flow signature in small systems (though not unexpected by all, see for example Ref. (54)) and the inability to determine if there was a contribution on the away-side underneath the dijet signal, there was speculation of possible new physics at play having nothing to do with the initial geometry followed by collective expansion. We discuss these alternative scenarios in Section 5.4.

In 2012, p +Pb collisions at $\sqrt{s_{NN}} = 5.02$ TeV were first run at the LHC and immediately all experiments published similar flow observations — see for example results from ALICE (55), ATLAS (56), and CMS (57). Here the experimental signatures were much stronger than in $p + p$ collisions and the race was on to repeat as many of the A+A measurements related to collectivity

to see if the signals persisted in p +Pb. Experimenters at RHIC immediately re-examined d +Au collision data at $\sqrt{s_{NN}} = 200$ GeV from 2008 and found similar patterns, though with a smaller flow signal relative to the non-flow backgrounds (58). To date, nearly all observations in A+A collisions that provided strong evidence for the standard “quark-gluon plasma as near-perfect fluid” model have now been measured in p +Pb and d +Au— see Ref. (59) for an excellent review. The notable exception to this statement is jet quenching, which is discussed in Section 5.1.

4.2. Instructive Measurements

Here we highlight four particularly instructive measurements in small systems, each of which tests a key aspect of extending the heavy ion standard model to these systems. These measurements involve (i) multi-particle cumulants that demonstrate that correlations exist amongst the majority of emitted particles as opposed to a small subset, (ii) manipulating the colliding small nuclei to see if the correlations scale as expected with initial geometry, (iii) particle-identified flow patterns to see if they reflect a common velocity field of a fluid at hadronization, and (iv) higher moments of the flow pattern including triangular and quadrangular flow.

4.2.1. Multi-particle cumulants. In a collision creating N particles, one can ask if a given two-particle correlation is indicative of correlations involving only a small subset of particles $M \ll N$ (as in the dijet case), or from $M \approx N$, i.e. a feature of the “bulk”. Most non-hydrodynamic explanations for the observations in small systems invoking finite-size momentum domains predicted the former case, while an overall flowing medium implies the latter case. Multi-particle cumulants utilize sets of 2, 4, 6, ..., n -particles which sequentially subtract away correlations amongst only $n-2$ particles, with an extension to all N particles using the Lee-Yang Zeros method (60, 61). These measurements have been particularly powerful since in the small-variance Gaussian limit the 2-particle and 4-particle results can be written as $v_2\{2\} = \sqrt{\bar{v}_2^2 + \sigma^2}$ and $v_2\{4\} \approx \sqrt{\bar{v}_2^2 - \sigma^2}$. They therefore allow extraction of both the event averaged \bar{v}_2 and the event-by-event variance σ^2 (62). This has established in A+A collisions at RHIC and the LHC a direct quantitative connection between the event-by-event variation in the initial geometry and the flow fluctuations(63).

Figure 3 shows v_2 multi-particle cumulants as measured in $p + p$, p +Pb, and Pb+Pb collisions at the LHC (64–68). The splitting of $v_2\{2\} > v_2\{4\}$, as related to flow fluctuations, is also seen in p +Pb collisions, yet disappears in the $p + p$ case. In 2016, RHIC had a special run of d +Au collisions over a range of energies (200, 62.4, 39, 19.6 GeV) to address how low in energy these features persist. The d +Au at 200 GeV results on the 2-, 4-, and 6-particle cumulants also indicate that the correlations are at the multi-particle level (69).

We note that non-zero multi-particle cumulants are not unique to a hydrodynamic description — see for example Refs. (59, 70). Imagine a flock of birds in flight that have N -body correlations, where

order can be the effect of a top-down centralized control mechanism (for example, due to the presence of one or more leaders), or it can be a bottom-up self-organized feature emerging from

local behavioral rules. The prominent difference between the centralized and the self-organized paradigm is not order, but response (71).

Thus, the key connection is the relation of cumulants to the response to initial geometry, rather than the mere real-valued v_2, v_4, v_6 , etc.

In summary, the multi-particle measurements in A+A, p +Pb, and d +Au collisions at RHIC and the LHC give strong evidence for N -body correlations, providing a connection to the fluctuating initial conditions. However, in the lower multiplicity cases of $p + p$ at the LHC, p +Au and lower energy d +Au at RHIC, the cumulants do not follow the expected small variance expectation, which may not be surprising as the fluctuations and non-flow effects are larger. More work will be needed (e.g., see (72)) to resolve these questions.

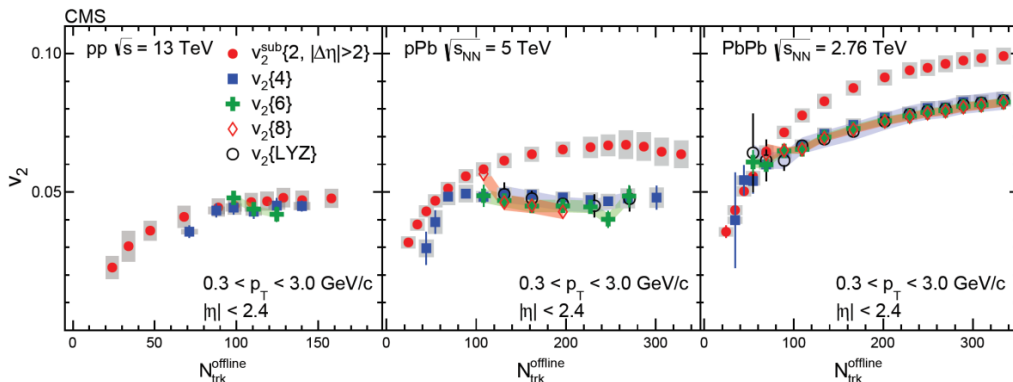


Figure 3

The v_2 multi-particle cumulants are shown as a function of charged particle multiplicity for $p + p$, p +Pb, and Pb+Pb collisions at the LHC (68).

4.2.2. Manipulating the Geometry. The initial small-system flow measurements at RHIC were made in d +Au collisions (58) rather than p +Au, due to accelerator constraints. However, it was noted that in a d +Au central collision, the projectile neutron and proton from the deuteron deposit energy in two hot spots thus giving a very different initial condition than the single hot spot in a p +Au collision (73). This key observation (74) led to a systematic program of “injecting” different initial-state asymmetries through p , d , and ^3He projectiles incident on Au nuclei at RHIC (75–77). As shown in Figure 4 (left panel), the various projectiles result in initial conditions that are dominantly circular, elliptical, and triangular for p , d , and ^3He projectiles respectively. Also shown in Figure 4 (right panel) are theoretical predictions from the hydrodynamic standard model (74) that are in excellent agreement with the subsequent experimental measurements of v_2 . In addition, the ^3He projectile was chosen to enhance triangular initial geometries and the

triangular flow v_3 has also been measured and is in agreement with theoretical predictions (76).

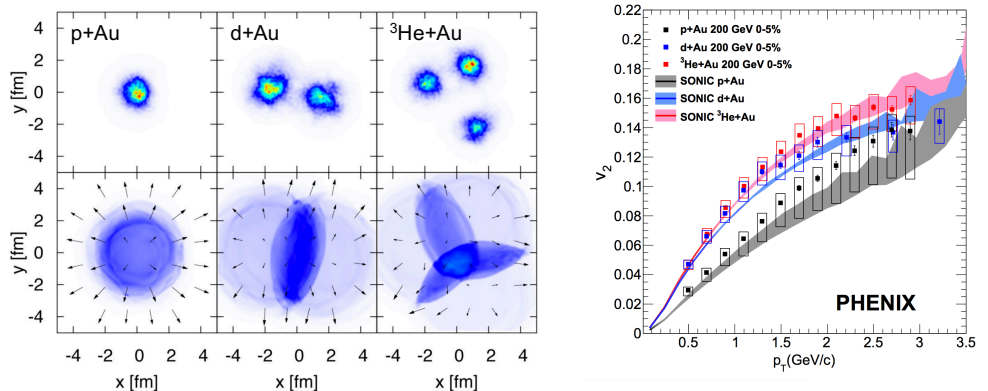


Figure 4

(left) Calculations of the initial energy density (top) in p +Au, d +Au, ^3He +Au collisions at RHIC and the resulting hydrodynamic evolution (below) (78); (right) Comparison of hydrodynamic calculations (74) to data from p +Au, d +Au and ^3He +Au collisions at $\sqrt{s_{NN}} = 200$ GeV (77).

The agreement with data requires a full modeling of both the initial conditions and the subsequent evolution. In the case of d +Au and ^3He +Au, the initial geometry is dominated by the location of the two or three-nucleons at the point of impact. In contrast, for p +Au, p +Pb, and in particular $p + p$ collisions, the initial geometry depends critically on the modeling of sub-nucleonic degrees of freedom – to be discussed in Section 5.2. The simultaneous description of the three engineered geometries at RHIC yields compelling evidence that the dominant correlation source can be related to initial geometry coupled with subsequent interactions or fluid dynamics. As of this writing no alternative explanation has been successfully put forward to describe these observations.

4.2.3. Mass-ordering “Fingerprint”. As noted in the A+A case, there is a distinct ordering of v_2 as a function of p_T for different hadron species. This ordering is often referred to as the “fingerprint” of a flowing fluid since it is the velocity of each fluid element as it hadronizes that results in different momentum boosts for the hadrons of different mass. Figure 5 shows the mass dependence of v_2 in $p + p$ (68), d +Au (75), and p +Pb (79) collisions, along with viscous hydrodynamic model comparisons in the latter two cases. The agreement of data and theory in the d +Au and p +Pb cases at RHIC and LHC energies is another check on the standard model.

4.2.4. Initial-State Fluctuations and Higher Moments. A big step forward in solidifying the standard model for A+A collisions was the incorporation of nucleon-level fluctuations for understand-

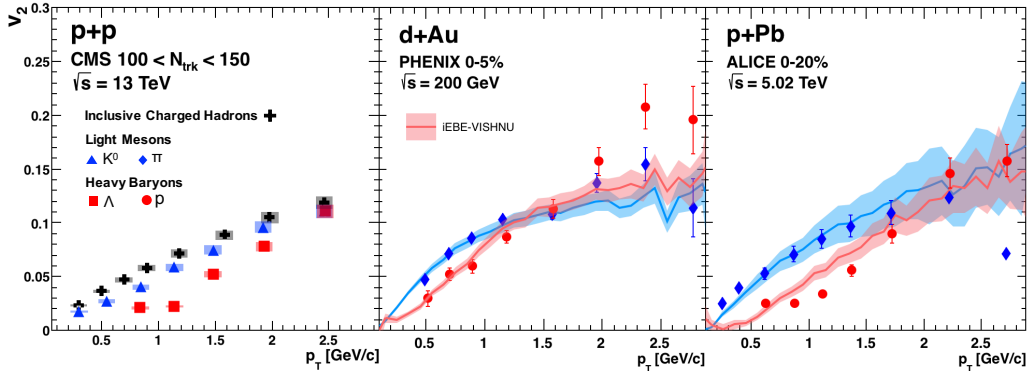


Figure 5

Elliptic flow coefficient v_2 as a function of p_T for different hadron species as measured in different small systems, $p + p$ at the LHC (left), $d + Au$ at RHIC (middle), and $p + Pb$ at the LHC (right). Theory calculations utilizing the hydrodynamic standard model are from Ref. (80).

ing the initial conditions and the resulting higher order flow coefficients. For $p + p$ and $p + Pb$ cases, sub-nucleon level fluctuations are crucial as discussed in Section 5.2. Figure 6 shows the measured v_2 , v_3 , and v_4 coefficients as a function of p_T in $p + p$, $p + Pb$, and $Pb + Pb$ central collisions at LHC energies (81). Also shown are calculations from the SONIC implementation of the standard model starting with initial conditions based on sub-nucleon structure and $\eta/s = 1/4\pi$. Within the unified framework of the heavy ion standard model, one achieves agreement for all three systems and for all orders of v_n .

4.3. Limits of Small System Flow Behavior

All of these results engender the question: how low in deposited energy, or in final particle multiplicity, does the experimental data exhibit correlations that match viscous hydrodynamic calculations? There are two different experimental ways to attack this question: (i) examining lower multiplicity $p + p$ interactions and (ii) examining small system collisions at lower energy. After the initial discovery of the $p + p$ “ridge” at the LHC in collisions at 0.9-7 TeV, follow-up measurements in $p + p$ collisions at higher energies of up to 13.1 TeV reveal an even stronger signal. However, for $p + p$ collisions of lower multiplicity, the non-flow contributions increase and a reliable extraction of the “flow” signal becomes model-dependent. ATLAS (53) and CMS (68) employ different extraction methods and currently come to different conclusions regarding when the flow signal disappears.

The other avenue to pursue this question is with the $d + Au$ beam energy scan at RHIC. In this case, one has better control over the initial geometry while changing the energy deposition and the total particle multiplicity, albeit with larger theoretical uncertainties due to the un-

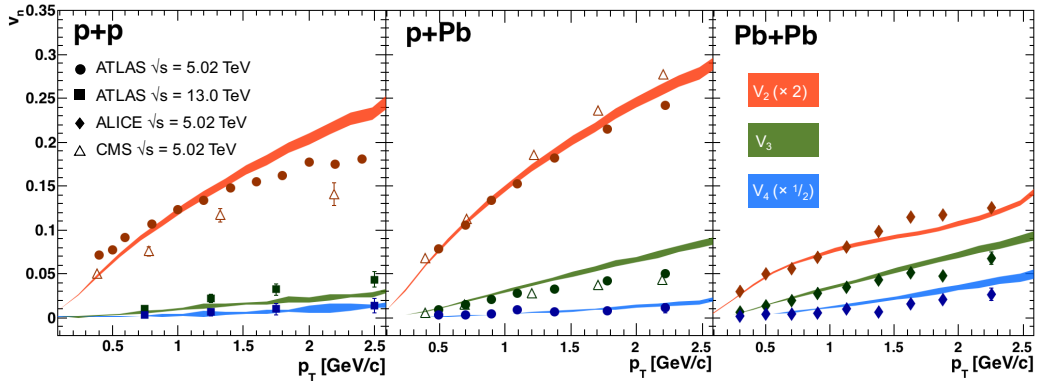


Figure 6

Experimental data for momentum anisotropies v_2, v_3, v_4 as a function of p_T in p + p, p+Pb, Pb+Pb collisions at the LHC. Also shown are hydrodynamic standard model (superSONIC) calculations that incorporate constituent quark Monte Carlo Glauber initial conditions, pre-equilibrium dynamics, viscous hydrodynamics with $\eta/s = 1/4\pi$, and hadronic scattering (81).

known variation of the transport coefficients and the equation of state with the increasing baryon chemical potential. Calculations within the hydrodynamic framework predicted a rather modest decrease in the flow signal (82, 83). Results from the PHENIX collaboration on v_2 as a function of collision energy (200, 62.4, 39, 19.6 GeV) have been reported (84). Figure 7 shows the measured v_2 coefficients as a function of pseudorapidity for high-multiplicity $d+Au$ collisions at the three higher energies. The measured v_2 shows little energy dependence, in reasonable agreement with hydrodynamic calculations. Also shown are parton transport model calculations that are detailed in Section 5.3. In $d+Au$ central collision data at 200 GeV, as noted earlier, there is additional evidence from the two-, four-, and six-particle cumulants that the anisotropy is a bulk N -particle correlation dominated by the translation of initial geometry into momentum space. The “flow” signal via cumulants appears to persist down to the lowest energies measured, though masked by a growing “non-flow” contribution to the correlations. The question of how small or low in energy these collective features persist remains outstanding and its resolution may hinge on whether one can perfectly factorize the flow and non-flow contributions.

5. Additional Considerations

There are a number of additional considerations that are important to include in any discussion of small system heavy ion physics. Here we include two key topics that must be reconciled when applying the heavy ion standard model to these small systems: 1) the apparent absence of jet quenching effects in small collision systems and 2) the influence of modeling the initial conditions at the sub-nucleonic level. In addition, there are proposed alternative interpretations of the

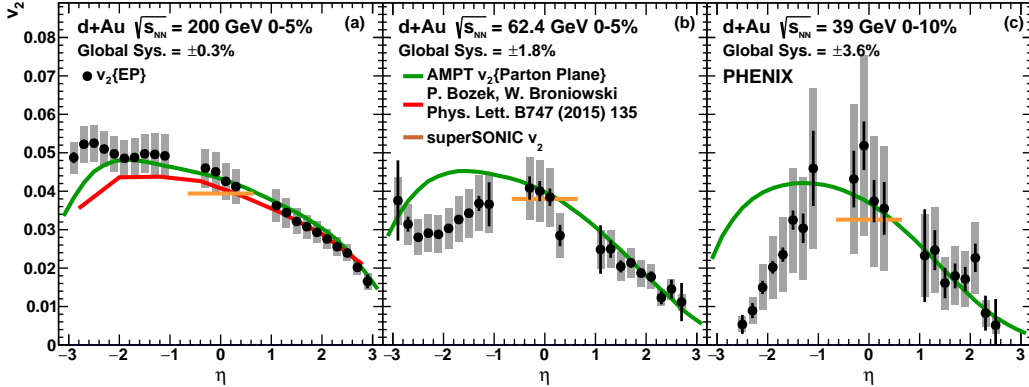


Figure 7

Measured v_2 integrated over p_T as a function of pseudorapidity is shown from $d+Au$ collisions at 200, 62.4, 39 GeV. Also, shown are calculations within the standard hydrodynamic framework (red and orange curves), as well as calculations from the parton and hadron transport framework (AMPT) detailed later in Section 5.3.

small system data that include (i) parton scattering models with well defined quasi-particles and (ii) initial state momentum correlation models. We detail these considerations in the next four subsections.

5.1. Absence of Jet Quenching in Small Collision Systems

In A+A collisions, an important confirmation of the standard model comes from the energy loss of high p_T partons traversing the medium, referred to as jet quenching (85–87). Jet quenching models calculate the rate and kinematics for hard scattering, i.e. large momentum-transfer interactions, and then propagate the resulting partons through the space-time evolution of the matter calculated from hydrodynamic codes. Jet quenching was discovered at RHIC in Au+Au collisions as a factor of five suppression of high p_T hadrons relative to their expected rate from scaling up $p+p$ yields (88). A critical measurement in 2003 was to see this “quenching” effect disappear in $d+Au$ collisions where no dense medium was expected (89, 90). No suppression was observed in $d+Au$ collisions and thus, at the time, jet quenching was confirmed as an exclusively final state effect from the medium in A+A collisions. Similar measurements at the LHC of single hadrons in Pb+Pb and $p+Pb$ shown in Figure 8 (left panel) (91) contrast the quenching observed in A+A and the lack of quenching in small systems. Modern measurements including fully reconstructed jets and jet structure provide further evidence for quenching related modifications in A+A collisions, but not in $p+A$.

It now may seem surprising that no jet quenching effect is apparent in $p+A$ collisions if indeed a hot medium is formed. How can there be a medium created that is described by hydrodynamics,

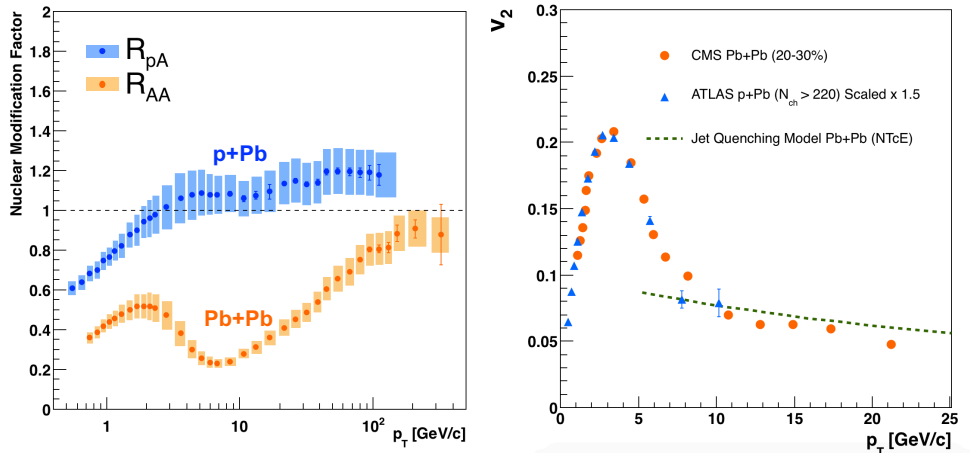


Figure 8

(left) The nuclear modification factor R_{AA} for unidentified hadrons as a function of p_T (91). This factor is the ratio of yields in A+A collisions relative to scaled up p + p yields. One observes significant modification, i.e. suppression, in Pb+Pb collisions and almost no modification in p+Pb collisions. (right) The v_2 coefficient for hadrons as a function of p_T in Pb+Pb and p+Pb collisions at the LHC. The p+Pb results have been scaled up by a factor of 1.5 for shape comparison. The theory curve (92) is from a jet quenching calculation where the anisotropy results from the directional dependence of the energy loss, rather than hydrodynamic flow.

and that significantly modifies the distribution of final state hadrons, yet has no significant impact on the distribution of high p_T particles? The jet quenching effect in A+A collisions becomes more prominent in more central, higher-multiplicity reactions as the average in-medium path the partons traverse correspondingly grows. In small systems, the medium created is smaller and thus the average path is expected to be significantly shorter. One speculation is that after the hard scattering, the parton is in a highly virtual state and its evolution may be only modestly affected by scattering with other partons in the medium. As such, a long medium traversal time as in central A+A collisions encompasses a parton where the medium scattering significantly modifies the parton shower, but in a p+A collision with short medium lifetimes $\tau < 2-4$ fm/c the jet quenching may be much smaller.

Quantitative theoretical calculations of the expected quenching effects in small systems have been made (see for example Refs. (92–94)), though no clear consensus on the magnitude of the quenching has been reached. The lack of quenching observed in Figure 8 (left panel) is seen in minimum bias collisions, i.e. averaged over all geometries. Many calculations predict observable quenching effects in central or high-multiplicity p+Pb collisions where the paths traversed by the partons may be longer. However, in these small systems, the selection of event classes based on multiplicity has strong autocorrelations between the nature of the nucleon-nucleon collisions

and the hard process itself, which complicate the interpretation of experimental observables. When selecting on multiplicity classes, jets and high- p_T hadrons are suppressed in so-called “central” events (as expected from jet quenching), but are counterbalanced by an equal magnitude enhancement in so-called “peripheral” events — thus resulting in no modification when averaging overall all $p+A$ collisions (95). The suppression in central events is widely interpreted in terms of this autocorrelation bias, i.e. pushing more events with jets into the most central category via multiplicity, rather than the result of jet quenching (96). Recent results with event class selected on spectator neutrons, and thus with reduced autocorrelation bias, indicate little or no quenching in more central event categories (97).

One mystery involves the measurement of v_2 for hadrons at large p_T . In the A+A case, the azimuthal anisotropy v_2 is interpreted in terms of flow for low p_T particles. In contrast at high p_T , hadrons have a more modest anisotropy in A+A collisions as shown in Figure 8. This anisotropy is thought to result from jet quenching, with partons losing more energy when traversing a longer path through the medium. What is striking is that the v_2 measured in $p+Pb$ (98) scaled by a factor of 1.5, as also shown in Figure 8 (right panel), appears to follow the same pattern. If there is no jet quenching in $p+Pb$ events, what else could be the source of the anisotropy at high p_T ?

Jet quenching is a fertile area of investigation and part of the motivation for comparing a full suite of jet measurements at RHIC from the new sPHENIX detector (99) to observations at the LHC over a range of collision system sizes. New measurements of charm and beauty hadrons in small systems are also expected to be illuminating. In A+A collisions, bulk medium hydrodynamics and rare jet quenching probes provide complementary information on the system created, and the presence of the former and apparent absence of the latter in small systems is a crucial area where more data and theoretical work is needed.

5.2. Initial Conditions

Extracting medium properties from hydrodynamic calculations relies on having a good quantitative constraint on the initial geometry. The simplest such geometry is calculated via the billiard ball interaction picture encapsulated in Monte Carlo Glauber calculations (100). Within this framework, individual nucleons are distributed within a nucleus following the relevant Woods-Saxon functional form and the inclusion of a hard-core repulsive potential. Nucleons in the projectile and target then interact as dictated by the nucleon-nucleon inelastic cross section. The resulting energy or entropy is distributed in the transverse plane according to a two-dimensional Gaussian with a width parameter typically chosen as $\sigma = 0.4$ fm. Extensions to this picture incorporate non-deterministic interaction probabilities, fluctuating nucleon sizes, and negative binomial fluctuations in energy deposition — see for example Refs. (101, 102).

In the case of A+A collisions, the (extended) nucleon-level Monte Carlo Glauber framework is, for the most part, sufficiently constrained to give confidence in the overall standard model space-time evolution and extraction of matter properties such as η/s with precision. This methodology was developed over many years and includes refinements such as the inclusion of deformation parameters, particularly for uranium, as well as detailed studies of nucleon-nucleon correlations.

In the case of $d+\text{Au}$ and ${}^3\text{He}+\text{Au}$ respectively, the Hulthen wavefunction for the deuteron is well understood and for ${}^3\text{He}$ the full three-body wavefunction has been solved *ab initio*. In these calculations, it has been shown that detailed substructure of the nucleon only influences results in the very most central A+A collisions where fluctuations are the dominant source of azimuthal anisotropies. However, in $p+p$ and proton-induced nuclear collisions, sub-nucleonic structure dominates and casts a shadow over the predictive power of the standard heavy ion modeling.

A number of studies of the influence of sub-nucleonic structure modeling have been carried out ((103, 104)), and here we describe two such studies. The first utilizes the so-called IP-Glasma framework, where the initial energy deposition is computed in terms of overlapping gluon fields. In this calculation the geometry of deposited energy follows the overlap regions between interacting nucleons, and thus in central $p+\text{Pb}$ and $p+\text{Au}$ collisions results in a very circular medium. This circular initial condition coupled with hydrodynamic evolution under-predicts the v_2 in $p+\text{Au}$ and $p+\text{Pb}$ by up to a factor of four. Thus, with very little initial eccentricity the medium simply expands radially with no strongly preferred axis. A second method utilizing the proton form-factor (105) also results in a very circular initial condition, and in particular for $p+p$ collisions predicts a vanishing v_2 for the highest multiplicity collisions. Models where the initial proton has deformations that fluctuate event-by-event can reconcile the $p+\text{Pb}$ data for example, but require additional parameters for each flow moment v_n (106) that potentially may be constrained from electron deep-inelastic scattering data.

Another approach is to include the simplest extension of the sub-nucleonic picture by assuming the proton is decomposed into three valence quarks each with a cloud of gluons around it, and that each “valence quark cloud” interacts when it comes within some fixed distance of another such “cloud.” In much of the literature this picture is referred to as the “constituent quark model.” The hydrodynamic calculation shown in Figure 6 gives a reasonable description of the v_2 , v_3 , and v_4 in $p+p$, $p+\text{Pb}$, $\text{Pb}+\text{Pb}$ collisions using this constituent quark Monte Carlo Glauber initial geometry. Further substructure, smaller than these “clouds”, is expected to have a small influence as a number of studies indicate that finer scale structures are very quickly washed out.

An intriguing new development is to invert the problem: if one posits viscous hydrodynamics as the correct model for the time evolution, then one can try to determine the initial condition and learn something about the structure of the proton on timescales that are short compared to the nucleus crossing time (104, 107). At RHIC energies, this may be feasible since one can test the hydrodynamic evolution hypothesis with $d+\text{Au}$ and ${}^3\text{He}+\text{Au}$ data that are not as sensitive to the initial condition model. There are also attempts to simultaneously constrain medium properties and initial condition substructure within a Bayesian framework (34–38). This is an exciting prospect and should be fully pursued for small system geometries at RHIC and the LHC.

5.3. Parton Transport Models

In the 1990’s parton transport models were developed which treated quarks and gluons as well-defined quasi-particles that scatter with each other. Early implementations such as VINI (108), ZPC (109, 110), and MPC (111) predicted rather modest collective effects (i.e. flow) due to the ex-

pected small QCD ($2 \rightarrow 2$) parton-parton scattering cross section. Had these calculations proved accurate, the produced medium could accurately be termed a weakly-coupled QGP. Instead, the first experimental data from RHIC with Au+Au collisions at $\sqrt{s_{NN}} = 130$ GeV indicating large elliptic flow immediately presented a major challenge for these frameworks. For example, within MPC, only by artificially increasing the expected pQCD parton-parton inelastic cross section from 3 mb to 45 mb, could one describe the data (112, 113). The conclusion at the time was that the medium is strongly coupled, i.e. the parton-parton interactions are highly non-perturbative and there are no well-defined quasi-particles. Thus the system is only amenable to calculations with strong fields or hydrodynamic descriptors.

However, a new class of parton transport models has been developed that provide a better qualitative description of experimental data. Two such examples are the BAMPS (114) and the AMPT (115) models. The BAMPS model considers only gluon quasi-particles subject to $gg \rightarrow gg$ scattering with a strong coupling $\alpha_s = 0.6$ as well as higher-order scattering of $gg \rightarrow ggg$ and $ggg \rightarrow gg$. In the limit of many scatterings, BAMPS produces hydrodynamic-like flow patterns and, within this framework, a small effective η/s value near the lowest bound is extracted (116).

A Multi-Phase Transport (AMPT) model (115) has nearly massless quark and anti-quark quasi-particles that are produced via a “string-melting” mechanism. The produced quarks are allowed to scatter, hadronize via coalescence, and then undergo hadronic inelastic and elastic scattering. The implementation of only quarks and anti-quarks enables a consistent recombination into hadrons via coalescence in the latter stage. This generator, though with many tunable components and various seemingly unphysical assumptions, e.g. no gluons, has successfully matched a number of A+A observables and provided insights into the translation of initial geometry into final hadron momentum anisotropies - most famously in Ref. (52). It was generally assumed that this was due to many scatterings that effectively modeled fluid flow, i.e. approaching the hydrodynamic limit as the mean free path approaches zero in the transport picture. However, recently it was shown that the number of scatterings is quite modest and for small systems at RHIC and the LHC the majority of partons have no scatterings at all. This realization has led to an understanding of the anisotropies as due to a differential probability to scatter or not — a so-called “parton escape” or “tomographic image” scenario (117). This puzzle is highlighted by the agreement (often quantitative) between AMPT and small system flow signals in p +Pb (118) and p +Au, d +Au, and ^3He +Au (119). An example of this agreement is shown in Figure 7 with calculations of v_2 as a function of pseudorapidity in d +Au collisions at different energies (84).

An important set of outstanding questions includes (i) are these parton quasi-particle scattering scenarios a dual picture to hydrodynamics even with very small scattering probability? and (ii) if not, are there key distinguishing experimental observables that can discriminate between the two? The latter question has been challenging to answer since many observables are sensitive to the initial geometry and fluctuations, yet rather insensitive to the mechanism of translation into momentum anisotropies. Thus, AMPT describes the v_2 , v_3 , v_4 and their fluctuations at the same level as hydrodynamics when utilizing the same initial conditions. Observables one naively would expect to be more sensitive such as the mass-dependent v_2 splitting are in fact qualitatively reproduced in AMPT yet result from completely different physics, in this case from the hadronic

scattering stage (120). Another observable is the correlation between flow moments, for example v_2 and v_4 , that arise in hydrodynamics from non-linear terms and hence mode mixing. However, AMPT calculations achieve a similar level of agreement with these mode-mixing observables (121).

These models are seemingly self-contradictory. Both AMPT and BAMPS have a short initial formation time for the partons to interact as well-defined quasi-particles and a mean free path between scatterings shorter than the de Broglie wavelength λ_{dBg} . In fact, in AMPT the initial parton formation time is approximately $0.2 \times \lambda_{dBg}$. Is it right to then say that a “weakly interacting” system of partons is an alternate picture to the “strongly coupled” hydrodynamics when setting $\alpha_s = 0.6$ and assuming mean free paths less than the de Broglie wavelength ($\lambda_{mfp} < \lambda_{dBg}$)? It is interesting to note that a precursor to the $\eta/s \geq 1/4\pi$ bound was in fact derived in kinetic theory assuming that a particle mean free path could not be shorter than the de Broglie wavelength (122). That said, the quantitative description of a large collection of experimental data implies that there is some key physics captured or mimicked in this approach. The field requires a concentrated effort in developing additional parton scattering models that are publicly available (as is AMPT), that simplify the physics assumptions to understand how to reconcile or discriminate this quasi-particle picture from the strongly-coupled hydrodynamic one.

5.4. Momentum Correlations Explanations

Both viscous hydrodynamics and parton transport calculations have a common feature: the initial geometry of the deposited energy in the transverse plane is translated into azimuthal momentum anisotropies via final-state interactions, either between fluid elements or quasi-particles. In contrast, when long-range “ridge” correlations were first reported in high-multiplicity p + p collisions at the LHC (51), explanations emerged where the correlations were generated in the initial scattering, i.e, on the time scale of the nuclear crossing, and required no later stage interactions or coupling. A number of these initial momentum correlation calculations are detailed in Ref. (123).

One proposal utilizes glasma graphs that produce correlated particles from different color flux tubes extended in rapidity with transverse separations less than the color-correlation length, $1/Q_s$, where Q_s is the saturation scale (124, 125). This picture results in back-to-back particle correlations, i.e. $\Delta\phi \approx 0, \pi$ that extend “long-range” in pseudorapidity. With a $Q_s \approx 1$ -2 GeV, the transverse length scale is 0.1-0.2 fm. Thus the correlation should exist only amongst a subset of the particles and the correlation should be predominantly back-to-back, resulting in a significant v_2 but no significant v_3 or higher moments. The measurement in small systems at RHIC and the LHC of multi-particle correlations and higher moment anisotropy coefficients present a challenge for these pictures. Recent work including additional diagrams indicate that these features may be recovered at a qualitative level, see Ref. (126) for a summary.

A key test of the momentum domain pictures comes from the geometry tests with p +Au, d +Au, ^3He +Au at RHIC. The momentum correlations originate in a local domain size of order 0.2 fm, which is quite small compared to the deuteron RMS diameter of 4.2 fm. Thus, a natural prediction of these locally generated correlations is that the signal should be smaller in d +Au collisions compared with p +Au. In the d +Au case, each domain is contained in only one local

“hot spot” originating from either the proton or neutron from the deuteron and thus the final correlation is diluted by the particles emitted from the other uncorrelated “hot spot.” In contrast, in the hydrodynamic picture the two “hot spots” evolve and merge thus generating a larger v_2 in the d +Au case. No successful explanation of this detailed geometry dependence exists to date from momentum domain calculations.

There are other momentum space explanations invoking color reconnection (127), radiating antennas (128), and target field anisotropy (129). More recently explanations invoking collectivity from interference (130) and color dipole orientation bias (131) have also been put forward. In most of these pictures the relation between small systems at RHIC and LHC is ignored, the relation of elliptic and triangular and quadrangular flow has no natural connection (in contrast to the case with initial geometry coupled with hydrodynamics), and the relation of $p + p$ to $p+A$ to $A+A$ is ad hoc or currently non-existent. Interestingly there is a recent attempt to gauge the combined influence of initial state momentum-domain correlations and final state scattering (132) modeled via BAMPS. To advance these alternatives there is no replacement for comprehensive calculations across energies, geometries, and observables.

6. Hydrodynamic Discussion and Implications

The modern view of hydrodynamics is to regard it as an effective theory which describes long wavelength excitations of a system after integrating out the microscopic degrees of freedom. The conserved charges of the theory in the simplest cases are simply the system’s four-momentum components, and the equations of motion are the conservation equations $\partial_\mu T^{\mu\nu} = 0$, where $T^{\mu\nu}$ is the stress-energy tensor. The fields can be taken as the fluid’s four-velocity u^μ and the energy density $\epsilon(T)$ (or alternatively the temperature T)². An equation of state specifying the pressure $p = p(\epsilon)$ as a function of energy density suffices to close this simple example. However, even for an ideal fluid described by $T_{ideal}^{\mu\nu} = (\epsilon + p)u^\mu u^\nu + pg^{\mu\nu}$ the equations of motion are clearly non-linear due to both the form of $T^{\mu\nu}$ and the constraint $u_\mu u^\mu = -1$ (here we take $c = 1$ and use the “mostly plus” metric convention standardly used in the relativistic hydrodynamic community).

Non-ideal behavior is typically separated from the ideal fluid contribution to the stress-energy tensor

$$T^{\mu\nu} = T_{ideal}^{\mu\nu} + \pi^{\mu\nu} \quad . \quad (3)$$

Working to first-order in a derivative expansion, in the local rest frame of the fluid defined by $u_{LFR}^\mu = (1, 0, 0, 0)$, the spatial components of $\pi^{\mu\nu}$ are parameterized as

$$\pi^{ij} = -\eta \left(\frac{\partial u^i}{\partial x^j} + \frac{\partial u^j}{\partial x^i} - \frac{2}{3} \delta^{ij} \partial_k u^k \right) - \zeta \partial_\mu u^\mu \quad , \quad (4)$$

where η and ζ are the shear and bulk viscosities, respectively. These expressions, while perfectly consistent with the definitions of viscosity for non-relativistic systems, lead to acausal behavior in

²For simplicity, we assume there are no other conserved charges with associated fields.

the relativistic equation of motion. Mathematically, this is because the kernel $\sim \exp[-x^2/(4\frac{\eta}{\epsilon+p}t)]$ is characteristic of parabolic diffusion equation; physically the super-luminal behavior is encoded in the assumption that the system can react instantaneously to a shear stress.

Müller(133) and then later Israel (134) and Israel-Stewart (135) developed a theory second-order in the gradient expansion that (at the linear level) preserved causality through the introduction of a relaxation time τ_{Π} for the non-equilibrium terms in the stress-energy tensor. This parameter may be viewed as a regulator for the effective theory (136) parameterizing the non-hydrodynamic (damped) modes necessary to ensure causality. As such, τ_{Π} is not an unbounded free parameter, as it must satisfy $\tau_{\Pi} > \eta/(\epsilon + p)$ to ensure linear perturbations in the sound channel do not exceed the speed of light (137). For a given system, it is necessary to determine whether the hydrodynamic modes dominate its description or whether there is a crucial dependence on the value of τ_{Π} indicating that the so-called nonhydrodynamic modes, i.e., the underlying physics of the regulator, are being studied(138, 139).

The necessity of the second-order term introduced by Müller-Israel-Stewart (MIS), together with the desire to apply hydrodynamics in small hadronic systems, requires understanding the order-by-order investigation of terms in the gradient expansion. The relevant expansion parameter in weakly coupled systems which admit a quasiparticle description is the Knudsen number ³ $K_N \equiv \ell_{mfp}/R$, as noted in Landau’s arguments in Section 2.

Simple estimates of parton mean free paths, under the assumption of the high parton density expected for a fully-developed QGP, provided only very modest support for the validity of a hydrodynamical description in small hadronic systems:

$$\ell_{mfp} \sim (2 \text{ fm}) \left(\frac{T_0}{T}\right)^3 \left(\frac{\sigma_1}{\sigma}\right) \quad , \quad (5)$$

where T is the temperature of the plasma in MeV, $T_0 = 200$ MeV (introduced to provide a scale; this is not the transition temperature), σ is the parton-parton cross section and $\sigma_1 = 1$ mb. Estimates such as Equation 5 have been used to argue that for collisions of large nuclei with radii $R \sim 6-7$ fm, parton-parton cross sections no larger than a few millibarns suffice to provide mean free paths significantly smaller than the system size, ensuring $K_N \leq 0.1$, down to temperatures of order 200 MeV or lower.

At the same time, it is clear that even for large nuclei, the separation of scales between ℓ_{mfp} and R is at best an order-of-magnitude. This observation engenders the question “What is the smallest drop of liquid QGP?” Two arguments suggest that a size as small as a femtometer might be plausible. First, the successes of hydrodynamics in describing the higher moments of the flow harmonics suggested circa 2010 that hydrodynamics was capable of describing features in the data with sizes $\sim R/n$, where n is the order of the flow harmonic. Second, the small value of η/s inferred from the data argued that the QGP must be strongly-coupled, suggesting that

³Again, this is a simplified description; a more general approach rooted in kinetic theory(139) allows for expansion in both K_N and the inverse Reynolds number $Re^{-1} \sim |\pi^{\mu\nu}|/p$, contravening Landau’s expectation that these are essentially the same in relativistic systems where hydrodynamics is applicable.

the ballistic transport assumptions used in the above expression for the mean free paths is an overestimate. Nonetheless the observation of flow-like features in p+A and p+p collisions were a surprising development to most researchers.

While the Müller-Israel-Stewart (MIS) theory was essential in establishing the possibility of relativistic causal theory of viscous hydrodynamics, it implemented only the minimal second-order term needed to eliminate superluminal behavior. The successes of the “Little Bang” model described in Section 3, and the attendant interest in reliably quantifying the key parameter $\frac{\eta}{s}$ motivated efforts to systematically investigate all allowed second-order terms.

In two remarkable papers(137, 140) remarkably submitted (independently) to the arXiv on the same day Baier, Romatschke, Son, Starinets and Stephanov (BRSSS), and Bhattacharyya, Hubeny, Minwalla and Rangamani (BHMR) used the gauge/gravity correspondence to not only investigate all five allowed second-order terms in a conformal theory of relativistic hydrodynamics but to also calculate the magnitude of the associated transport coefficients for a strongly-coupled system with the minimal value of $\frac{\eta}{s}$, in particular finding $\tau_{\Pi} = \frac{2-\ln 2}{2\pi T} \approx \frac{1.31}{2\pi T} \approx \frac{0.21}{T}$. Romatschke extended this work to the case of non-conformal hydrodynamics (141), in which case there are 15 second-order terms, each with an associated transport coefficient. Further efforts led to gradient expansions to all orders in linearized theory (142); and “only” third-order in full theory (143).

These developments led to a greatly increased understanding of relativistic hydrodynamics with important consequences for evaluating its applicability in nuclear collisions in general, and small systems in particular, in which gradients are large. There is now a vast literature on the topic, drawing insights from kinetic theory, linear response theory and the gauge/gravity duality; for thorough and masterful reviews we refer the reader to Refs. (28, 144). Here we summarize the important conclusions from those efforts:

1. The success of viscous relativistic hydrodynamics in describing the bulk features, in particular the v_n 's does not necessarily imply that the matter is near thermal equilibrium during its hydrodynamic evolution. Rather, it is likely that high energy nuclear collisions remain out of equilibrium up to hadronization (30). Obviously, by definition hydrodynamics must be capable of addressing arbitrarily small perturbations about local equilibrium, but recent work has shown that this is also true in the case of momentum anisotropies of order one.
2. The key condition for the applicability of hydrodynamics in small systems is the dominance of hydrodynamics modes over non-hydrodynamic modes. This appears to be a tautological statement, but it can be put on a firm basis. Hydrodynamic modes have dispersion relations satisfying $\lim_{|\mathbf{k}| \rightarrow 0} \omega(\mathbf{k}) = 0$ consistent with the existence of conserved “charges” central to the defining equations. Conversely, non-hydrodynamic modes are those with finite imaginary values of $\omega(\mathbf{k})$ as \mathbf{k} goes to zero, indicative of transient behavior not captured in the hydrodynamic gradient expansion. Closely related to this observation is the divergence of that gradient expansion(145, 146), reflecting its inability to capture the non-hydrodynamic modes. The non-hydrodynamic modes are an essential part of the early time dynamics necessary to insure consistency and/or causality, but their late-time contributions to the dynamics should be small for hydrodynamics to apply.

3. All studies to date (28) indicate that the first 2-3 orders of the gradient expansion provide a very accurate description of a universal hydrodynamic attractor behavior(147) for $w \equiv \tau T_{eff}(\tau) > \sim 0.7$ (148), where τ is the time from the initial collision and $T_{eff}(\tau)$ is the *effective* temperature at that time as determined from the energy or entropy density. This is true even for systems that are grossly out of equilibrium, i.e., have momentum anisotropies of order one.
4. These considerations have led to the concept of a *hydrodynamization* time, ⁴ in analogy to the (not necessarily relevant) thermalization time, and defined as the time when the hydrodynamic modes dominate the system's behavior. All indications are that this time is of order $\tau_{Hydro} \sim (0.5-1.0) \frac{1}{T_{eff}(\tau)}$. Note that at this time first-order corrections to ideal hydrodynamics can still be large, but the subsequent evolution is well-described by viscous relativistic hydrodynamics.
5. The requirement that the hydrodynamic modes dominate non-hydrodynamic effects resulting from the second-order transport coefficient τ_{Π} can be used to obtain a criterion on the smallest system expected to exhibit hydrodynamic behavior. Three semi-independent lines of reasoning (105, 136, 152) lead to the surprising that charged-particle rapidity densities satisfying $\frac{dN_{ch}}{dy} > 2-4$ suffice for a valid description of system evolution using viscous relativistic hydrodynamics.

To summarize, there are ample theoretical arguments developed over the past decade to suggest that viscous relativistic hydrodynamics can be applied to describe particle production and flow in p+p and p+A collisions at high energies. There is strong internal consistency in this reasoning. The arguments (for the large part) rely on strong-coupling, which in turn implies a small value of $\frac{\eta}{s}$, which when used in hydrodynamics modeling results in good agreement with the data. Similarly, the criterion that $\ell_{mfp} \sim \frac{1}{T}$ for minimal viscosity systems (122) is echoed in the observation (153, 154) that under these conditions a plausible bound on the minimum system size R for a hydrodynamic description is $R \sim \frac{1}{T_{eff}}$, which is supported by numerical studies in the dual gravity system(155, 156). Further support is provided by the preservation of structure in the final state in A+A collisions up to at least v_5 , which in effect are feature sizes of order 1/5 those of the nuclear size.

7. Summary

In summary, as of this writing the field of relativistic heavy ion physics is in the midst of a revolution in our understanding of the conditions necessary for nuclear matter to behave as a near-perfect fluid with bulk dynamics described by viscous relativistic hydrodynamics. The implications of this revolution extend to other many-body strongly coupled systems and the conditions necessary for hydrodynamic description.

⁴In an interesting example of confluence, this awkward but accurate construct first appeared in an August, 2013 paper on astrophysical plasmas (149) and then in in the heavy ion context in October of the same year (150) and three weeks later in (151).

DISCLOSURE STATEMENT

The authors are not aware of any affiliations, memberships, funding, or financial holdings that might be perceived as affecting the objectivity of this review.

ACKNOWLEDGMENTS

We are pleased to acknowledge very useful comments from Jorge Noronha, Jaki Noronha-Hostler, Constantin Loizides, Krishna Rajagopal and Paul Romatschke. We also acknowledge work on the graphics by Javier Orjuela-Koop. JLN and WAZ acknowledge funding from the Division of Nuclear Physics of the U.S. Department of Energy grants DE-FG02-00ER41152 and DE-FG02-86ER40281, respectively.

LITERATURE CITED

1. N. Bohr, *Neutron Capture and Nuclear Constitution*, Nature **137** (1936) 344–348.
2. R. H. Stuewer, *The origin of the liquid-drop model and the interpretation of nuclear fission*, Perspectives on Science **2** (1994) 76–129.
3. N. Bohr and J. A. Wheeler, *The Mechanism of nuclear fission*, Phys. Rev. **56** (1939) 426–450.
4. W. Heisenberg, *Production of Meson Showers*, Nature **164** (1949) 65–66.
5. E. Fermi, *High-energy nuclear events*, Prog. Theor. Phys. **5** (1950) 570–583.
6. E. Fermi, *Collected Papers:(Note E Memorie).*, Collected Papers **Vol. 2** (1962) .
7. L. D. Landau, *On the multiparticle production in high-energy collisions*, Izv. Akad. Nauk Ser. Fiz. **17** (1953) 51–64.
8. I. Ya. Pomeranchuk, *On the theory of multiple particle production in a single collision*, Dokl. Akad. Nauk Ser. Fiz. **78** (1951) 889–891.
9. S. Z. Belenkij and L. D. Landau, *Hydrodynamic theory of multiple production of particles*, Nuovo Cim. Suppl. **3S10** (1956) 15. [Usp. Fiz. Nauk56,309(1955)].
10. P. Carruthers and M. Doung-van, *Rapidity and angular distributions of charged secondaries according to the hydrodynamical model of particle production*, Phys. Rev. **D8** (1973) 859–874.
11. J. D. Bjorken, *Highly Relativistic Nucleus-Nucleus Collisions: The Central Rapidity Region*, Phys. Rev. **D27** (1983) 140–151.
12. E735, T. Alexopoulos et al., *Mass identified particle production in $p\bar{p}$ collisions at $\sqrt{s} = 300\text{-GeV}$, 540-GeV , 1000-GeV , and 1800-GeV* , Phys. Rev. **D48** (1993) 984–997.
13. MiniMax, T. C. Brooks et al., *A Search for disoriented chiral condensate at the Fermilab Tevatron*, Phys. Rev. **D61** (2000) 032003, [arXiv:hep-ex/9906026](#) [hep-ex].
14. ALICE, J. Adam et al., *Enhanced production of multi-strange hadrons in high-multiplicity proton-proton collisions*, Nature Phys. **13** (2017) 535–539, [arXiv:1606.07424](#) [nucl-ex].
15. PHENIX, K. Adcox et al., *Formation of dense partonic matter in relativistic nucleus-nucleus collisions at RHIC: Experimental evaluation by the PHENIX collaboration*, Nucl. Phys. **A757** (2005) 184–283, [arXiv:nucl-ex/0410003](#) [nucl-ex].
16. STAR, J. Adams et al., *Experimental and theoretical challenges in the search for the quark gluon plasma: The STAR Collaboration’s critical assessment of the evidence from RHIC collisions*, Nucl. Phys. **A757** (2005) 102–183, [arXiv:nucl-ex/0501009](#) [nucl-ex].

17. B. B. Back et al., *The PHOBOS perspective on discoveries at RHIC*, Nucl. Phys. **A757** (2005) 28–101, [arXiv:nuc1-ex/0410022 \[nucl-ex\]](#).
18. BRAHMS, I. Arsene et al., *Quark gluon plasma and color glass condensate at RHIC? The Perspective from the BRAHMS experiment*, Nucl. Phys. **A757** (2005) 1–27, [arXiv:nuc1-ex/0410020 \[nucl-ex\]](#).
19. P. Kovtun, D. T. Son, and A. O. Starinets, *Viscosity in strongly interacting quantum field theories from black hole physics*, Phys. Rev. Lett. **94** (2005) 111601, [arXiv:hep-th/0405231 \[hep-th\]](#).
20. D. T. Son and A. O. Starinets, *Viscosity, Black Holes, and Quantum Field Theory*, Ann. Rev. Nucl. Part. Sci. **57** (2007) 95–118, [arXiv:0704.0240 \[hep-th\]](#).
21. B. Muller, J. Schukraft, and B. Wyslouch, *First Results from Pb+Pb collisions at the LHC*, Ann. Rev. Nucl. Part. Sci. **62** (2012) 361–386, [arXiv:1202.3233 \[hep-ex\]](#).
22. ALICE, J. Adam et al., *Direct photon production in Pb-Pb collisions at 2.76 TeV*, Phys. Lett. **B754** (2016) 235–248, [arXiv:1509.07324 \[nucl-ex\]](#).
23. P. Romatschke, *New Developments in Relativistic Viscous Hydrodynamics*, Int. J. Mod. Phys. **E19** (2010) 1–53, [arXiv:0902.3663 \[hep-ph\]](#).
24. U. Heinz and R. Snellings, *Collective flow and viscosity in relativistic heavy-ion collisions*, Ann. Rev. Nucl. Part. Sci. **63** (2013) 123–151, [arXiv:1301.2826 \[nucl-th\]](#).
25. S. Jeon and U. Heinz, *Introduction to Hydrodynamics*, Int. J. Mod. Phys. **E24** (2015) no. 10, 1530010, [arXiv:1503.03931 \[hep-ph\]](#).
26. A. Jaiswal and V. Roy, *Relativistic hydrodynamics in heavy-ion collisions: general aspects and recent developments*, Adv. High Energy Phys. **2016** (2016) 9623034, [arXiv:1605.08694 \[nucl-th\]](#).
27. H. Song, Y. Zhou, and K. Gajdosova, *Collective flow and hydrodynamics in large and small systems at the LHC*, Nucl. Sci. Tech. **28** (2017) no. 7, 99, [arXiv:1703.00670 \[nucl-th\]](#).
28. W. Florkowski, M. P. Heller, and M. Spalinski, *New theories of relativistic hydrodynamics in the LHC era*, [arXiv:1707.02282 \[hep-ph\]](#).
29. P. Romatschke, *Far From Equilibrium Fluid Dynamics*, [arXiv:1704.08699 \[hep-th\]](#).
30. P. Romatschke, *Do nuclear collisions create a locally equilibrated quark–gluon plasma?*, Eur. Phys. J. **C77** (2017) no. 1, 21, [arXiv:1609.02820 \[nucl-th\]](#).
31. Y. Aoki, G. Endrodi, Z. Fodor, S. D. Katz, and K. K. Szabo, *The Order of the quantum chromodynamics transition predicted by the standard model of particle physics*, Nature **443** (2006) 675–678, [arXiv:hep-lat/0611014 \[hep-lat\]](#).
32. Y. Aoki, S. Borsanyi, S. Durr, Z. Fodor, S. D. Katz, S. Krieg, and K. K. Szabo, *The QCD transition temperature: results with physical masses in the continuum limit II.*, JHEP **06** (2009) 088, [arXiv:0903.4155 \[hep-lat\]](#).
33. F. Cooper and G. Frye, *Comment on the Single Particle Distribution in the Hydrodynamic and Statistical Thermodynamic Models of Multiparticle Production*, Phys. Rev. **D10** (1974) 186.
34. H. Petersen, C. Coleman-Smith, S. A. Bass, and R. Wolpert, *Constraining the initial state granularity with bulk observables in Au+Au collisions at $\sqrt{s_{NN}} = 200$ GeV*, J. Phys. **G38** (2011) 045102, [arXiv:1012.4629 \[nucl-th\]](#).
35. J. Novak, K. Novak, S. Pratt, J. Vredevoogd, C. Coleman-Smith, and R. Wolpert, *Determining Fundamental Properties of Matter Created in Ultrarelativistic Heavy-Ion Collisions*, Phys. Rev. **C89** (2014) no. 3, 034917, [arXiv:1303.5769 \[nucl-th\]](#).
36. S. Pratt, E. Sangaline, P. Sorensen, and H. Wang, *Constraining the Eq. of State of Super-Hadronic Matter from Heavy-Ion Collisions*, Phys. Rev. Lett. **114** (2015) 202301, [arXiv:1501.04042 \[nucl-th\]](#).

37. J. E. Bernhard, J. S. Moreland, S. A. Bass, J. Liu, and U. Heinz, *Applying Bayesian parameter estimation to relativistic heavy-ion collisions: simultaneous characterization of the initial state and quark-gluon plasma medium*, Phys. Rev. **C94** (2016) no. 2, 024907, [arXiv:1605.03954](#) [nucl-th].
38. J. S. Moreland, J. E. Bernhard, W. Ke, and S. A. Bass, *Flow in small and large quark-gluon plasma droplets: the role of nucleon substructure*, in *26th International Conference on Ultrarelativistic Nucleus-Nucleus Collisions (Quark Matter 2017) Chicago, Illinois, USA, February 6-11, 2017*. 2017. [arXiv:1704.04486](#) [nucl-th].
<https://inspirehep.net/record/1591644/files/arXiv:1704.04486.pdf>.
39. J.-Y. Ollitrault, *Anisotropy as a signature of transverse collective flow*, Phys. Rev. **D46** (1992) 229–245.
40. S. Voloshin and Y. Zhang, *Flow study in relativistic nuclear collisions by Fourier expansion of Azimuthal particle distributions*, Z. Phys. **C70** (1996) 665–672, [arXiv:hep-ph/9407282](#) [hep-ph].
41. C. Gale, S. Jeon, B. Schenke, P. Tribedy, and R. Venugopalan, *Event-by-event anisotropic flow in heavy-ion collisions from combined Yang-Mills and viscous fluid dynamics*, Phys. Rev. Lett. **110** (2013) no. 1, 012302, [arXiv:1209.6330](#) [nucl-th].
42. C. Shen, U. Heinz, P. Huovinen, and H. Song, *Radial and elliptic flow in Pb+Pb collisions at the Large Hadron Collider from viscous hydrodynamic*, Phys. Rev. **C84** (2011) 044903, [arXiv:1105.3226](#) [nucl-th].
43. N. Borghini, P. M. Dinh, and J.-Y. Ollitrault, *A New method for measuring azimuthal distributions in nucleus-nucleus collisions*, Phys. Rev. **C63** (2001) 054906, [arXiv:nucl-th/0007063](#) [nucl-th].
44. M. A. Lisa, S. Pratt, R. Soltz, and U. Wiedemann, *Femtoscopy in relativistic heavy ion collisions*, Ann. Rev. Nucl. Part. Sci. **55** (2005) 357–402, [arXiv:nucl-ex/0505014](#) [nucl-ex].
45. D. Teaney and L. Yan, *Non linearities in the harmonic spectrum of heavy ion collisions with ideal and viscous hydrodynamics*, Phys. Rev. **C86** (2012) 044908, [arXiv:1206.1905](#) [nucl-th].
46. S. Pratt, *Resolving the HBT Puzzle in Relativistic Heavy Ion Collision*, Phys. Rev. Lett. **102** (2009) 232301, [arXiv:0811.3363](#) [nucl-th].
47. C. Shen, Z. Qiu, and U. Heinz, *Shape and flow fluctuations in ultracentral Pb + Pb collisions at the energies available at the CERN Large Hadron Collider*, Phys. Rev. **C92** (2015) no. 1, 014901, [arXiv:1502.04636](#) [nucl-th].
48. PHENIX, A. Adare et al., *Azimuthally anisotropic emission of low-momentum direct photons in Au+Au collisions at $\sqrt{s_{NN}} = 200$ GeV*, Phys. Rev. **C94** (2016) no. 6, 064901, [arXiv:1509.07758](#) [nucl-ex].
49. C. A. Salgado and J. P. Wessels, *Proton-Lead Collisions at the CERN LHC*, Ann. Rev. Nucl. Part. Sci. **66** (2016) 449–473.
50. K. J. Eskola, H. Paukkunen, and C. A. Salgado, *EPS09: A New Generation of NLO and LO Nuclear Parton Distribution Functions*, JHEP **04** (2009) 065, [arXiv:0902.4154](#) [hep-ph].
51. CMS, V. Khachatryan et al., *Observation of Long-Range Near-Side Angular Correlations in Proton-Proton Collisions at the LHC*, JHEP **09** (2010) 091, [arXiv:1009.4122](#) [hep-ex].
52. B. Alver and G. Roland, *Collision geometry fluctuations and triangular flow in heavy-ion collisions*, Phys. Rev. **C81** (2010) 054905, [arXiv:1003.0194](#) [nucl-th]. [Erratum: Phys. Rev. **C82**, 039903(2010)].
53. ATLAS, G. Aad et al., *Observation of Long-Range Elliptic Azimuthal Anisotropies in $\sqrt{s} = 13$ and 2.76 TeV pp Collisions with the ATLAS Detector*, Phys. Rev. Lett. **116** (2016) no. 17, 172301, [arXiv:1509.04776](#) [hep-ex].
54. P. Bozek, *Collective flow in p-Pb and d-Pd collisions at TeV energies*, Phys. Rev. **C85** (2012)

- 014911, [arXiv:1112.0915 \[hep-ph\]](#).
55. ALICE, B. Abelev et al., *Long-range angular correlations on the near and away side in p-Pb collisions at $\sqrt{s_{NN}} = 5.02$ TeV*, Phys. Lett. **B719** (2013) 29–41, [arXiv:1212.2001 \[nucl-ex\]](#).
 56. ATLAS, G. Aad et al., *Observation of Associated Near-Side and Away-Side Long-Range Correlations in $\sqrt{s_{NN}}=5.02$ TeV Proton-Lead Collisions with the ATLAS Detector*, Phys. Rev. Lett. **110** (2013) no. 18, 182302, [arXiv:1212.5198 \[hep-ex\]](#).
 57. CMS, S. Chatrchyan et al., *Observation of long-range near-side angular correlations in proton-lead collisions at the LHC*, Phys. Lett. **B718** (2013) 795–814, [arXiv:1210.5482 \[nucl-ex\]](#).
 58. PHENIX, A. Adare et al., *Quadrupole Anisotropy in Dihadron Azimuthal Correlations in Central d+Au Collisions at $\sqrt{s_{NN}}=200$ GeV*, Phys. Rev. Lett. **111** (2013) no. 21, 212301, [arXiv:1303.1794 \[nucl-ex\]](#).
 59. C. Loizides, *Experimental overview on small collision systems at the LHC*, Nucl. Phys. **A956** (2016) 200–207, [arXiv:1602.09138 \[nucl-ex\]](#).
 60. R. S. Bhalerao, N. Borghini, and J. Y. Ollitrault, *Analysis of anisotropic flow with Lee-Yang zeroes*, Nucl. Phys. **A727** (2003) 373–426, [arXiv:nucl-th/0310016 \[nucl-th\]](#).
 61. N. Borghini, R. S. Bhalerao, and J. Y. Ollitrault, *Anisotropic flow from Lee-Yang zeroes: A Practical guide*, J. Phys. **G30** (2004) S1213–S1216, [arXiv:nucl-th/0402053 \[nucl-th\]](#).
 62. J.-Y. Ollitrault, A. M. Poskanzer, and S. A. Voloshin, *Effect of flow fluctuations and nonflow on elliptic flow methods*, Phys. Rev. **C80** (2009) 014904, [arXiv:0904.2315 \[nucl-ex\]](#).
 63. G. Giacalone, J. Noronha-Hostler, and J.-Y. Ollitrault, *Relative flow fluctuations as a probe of initial state fluctuations*, Phys. Rev. **C95** (2017) no. 5, 054910, [arXiv:1702.01730 \[nucl-th\]](#).
 64. ATLAS, G. Aad et al., *Measurement with the ATLAS detector of multi-particle azimuthal correlations in p+Pb collisions at $\sqrt{s_{NN}} = 5.02$ TeV*, Phys. Lett. **B725** (2013) 60–78, [arXiv:1303.2084 \[hep-ex\]](#).
 65. CMS, S. Chatrchyan et al., *Multiplicity and transverse momentum dependence of two- and four-particle correlations in pPb and PbPb collisions*, Phys. Lett. **B724** (2013) 213–240, [arXiv:1305.0609 \[nucl-ex\]](#).
 66. ALICE, B. B. Abelev et al., *Multiparticle azimuthal correlations in p-Pb and Pb-Pb collisions at the CERN Large Hadron Collider*, Phys. Rev. **C90** (2014) no. 5, 054901, [arXiv:1406.2474 \[nucl-ex\]](#).
 67. CMS, V. Khachatryan et al., *Evidence for Collective Multiparticle Correlations in p-Pb Collisions*, Phys. Rev. Lett. **115** (2015) no. 1, 012301, [arXiv:1502.05382 \[nucl-ex\]](#).
 68. CMS, V. Khachatryan et al., *Evidence for collectivity in pp collisions at the LHC*, Phys. Lett. **B765** (2017) 193–220, [arXiv:1606.06198 \[nucl-ex\]](#).
 69. PHENIX, C. Aidala et al., *Measurements of multiparticle correlations in d+Au collisions at 200, 62.4, 39, and 19.6 GeV and p+Au collisions at 200 GeV and implications for collective behavior*, [arXiv:1707.06108 \[nucl-ex\]](#).
 70. K. Dusling, M. Mace, and R. Venugopalan, *Parton model description of multiparticle azimuthal correlations in pA collisions*, [arXiv:1706.06260 \[hep-ph\]](#).
 71. A. Cavagna, A. Cimarelli, I. Giardina, G. Parisi, R. Santagati, F. Stefanini, and M. Viale, *Scale-free correlations in starling flocks*, Proceedings of the National Academy of Sciences **107** (2010) no. 26, 11865–11870, <http://www.pnas.org/content/107/26/11865.full.pdf>, <http://www.pnas.org/content/107/26/11865.abstract>.
 72. J. Jia, M. Zhou, and A. Trzupek, *Revealing long-range multiparticle collectivity in small collision systems via subevent cumulants*, Phys. Rev. **C96** (2017) no. 3, 034906, [arXiv:1701.03830](#)

[nucl-th].

73. PHENIX, A. Adare et al., *Centrality categorization for $R_{p(d)+A}$ in high-energy collisions*, Phys. Rev. **C90** (2014) no. 3, 034902, [arXiv:1310.4793](#) [nucl-ex].
74. J. L. Nagle, A. Adare, S. Beckman, T. Koblesky, J. Orjuela Koop, D. McGlinchey, P. Romatschke, J. Carlson, J. E. Lynn, and M. McCumber, *Exploiting Intrinsic Triangular Geometry in Relativistic He3+Au Collisions to Disentangle Medium Properties*, Phys. Rev. Lett. **113** (2014) no. 11, 112301, [arXiv:1312.4565](#) [nucl-th].
75. PHENIX, A. Adare et al., *Measurement of long-range angular correlation and quadrupole anisotropy of pions and (anti)protons in central d+Au collisions at $\sqrt{s_{NN}}=200$ GeV*, Phys. Rev. Lett. **114** (2015) no. 19, 192301, [arXiv:1404.7461](#) [nucl-ex].
76. PHENIX, A. Adare et al., *Measurements of elliptic and triangular flow in high-multiplicity $^3\text{He}+Au$ collisions at $\sqrt{s_{NN}} = 200$ GeV*, Phys. Rev. Lett. **115** (2015) no. 14, 142301, [arXiv:1507.06273](#) [nucl-ex].
77. C. Aidala et al., *Measurement of long-range angular correlations and azimuthal anisotropies in high-multiplicity p+Au collisions at $\sqrt{s_{NN}} = 200$ GeV*, Phys. Rev. **C95** (2017) no. 3, 034910, [arXiv:1609.02894](#) [nucl-ex].
78. A. Aprahamian et al., *Reaching for the horizon: The 2015 long range plan for nuclear science, 2015*. https://science.energy.gov/~media/np/nsac/pdf/2015LRP/2015_LRPNS_091815.pdf.
79. ALICE, B. B. Abelev et al., *Long-range angular correlations of π , K and p in p-Pb collisions at $\sqrt{s_{NN}} = 5.02$ TeV*, Phys. Rev. Lett. **B726** (2013) 164–177, [arXiv:1307.3237](#) [nucl-ex].
80. C. Shen, J.-F. Paquet, G. S. Denicol, S. Jeon, and C. Gale, *Collectivity and electromagnetic radiation in small systems*, Phys. Rev. **C95** (2017) no. 1, 014906, [arXiv:1609.02590](#) [nucl-th].
81. R. D. Weller and P. Romatschke, *One fluid to rule them all: viscous hydrodynamic description of event-by-event central p+p, p+Pb and Pb+Pb collisions at $\sqrt{s} = 5.02$ TeV*, Phys. Lett. **B774** (2017) 351–356, [arXiv:1701.07145](#) [nucl-th].
82. P. Romatschke, *Light-Heavy Ion Collisions: A window into pre-equilibrium QCD dynamics?*, Eur. Phys. J. **C75** (2015) no. 7, 305, [arXiv:1502.04745](#) [nucl-th].
83. J. D. Orjuela Koop, R. Belmont, P. Yin, and J. L. Nagle, *Exploring the Beam Energy Dependence of Flow-Like Signatures in Small System d+Au Collisions*, Phys. Rev. **C93** (2016) no. 4, 044910, [arXiv:1512.06949](#) [nucl-th].
84. PHENIX, C. Aidala et al., *Measurements of azimuthal anisotropy and charged-particle multiplicity in d+Au collisions at $\sqrt{s_{NN}} = 200, 62.4, 39,$ and 19.6 GeV*, [arXiv:1708.06983](#) [nucl-ex].
85. M. Gyulassy, I. Vitev, X.-N. Wang, and B.-W. Zhang, *Jet quenching and radiative energy loss in dense nuclear matter*, [arXiv:nucl-th/0302077](#) [nucl-th].
86. E. Norbeck, K. Šafařík, and P. A. Steinberg, *Hard-Scattering Results in Heavy-Ion Collisions at the LHC*, Ann. Rev. Nucl. Part. Sci. **64** (2014) 383–411.
87. A. Accardi, F. Arleo, W. K. Brooks, D. D’Enterria, and V. Muccifora, *Parton Propagation and Fragmentation in QCD Matter*, Riv. Nuovo Cim. **32** (2010) 439–553, [arXiv:0907.3534](#) [nucl-th].
88. PHENIX, K. Adcox et al., *Suppression of hadrons with large transverse momentum in central Au+Au collisions at $\sqrt{s_{NN}} = 130$ -GeV*, Phys. Rev. Lett. **88** (2002) 022301, [arXiv:nucl-ex/0109003](#) [nucl-ex].
89. STAR, J. Adams et al., *Evidence from d + Au measurements for final state suppression of high $p(T)$ hadrons in Au+Au collisions at RHIC*, Phys. Rev. Lett. **91** (2003) 072304, [arXiv:nucl-ex/0306024](#) [nucl-ex].
90. PHENIX, S. S. Adler et al., *Absence of suppression in particle production at large transverse*

- momentum in $S(NN)^{1/2} = 200\text{-GeV } d + Au$ collisions, Phys. Rev. Lett. **91** (2003) 072303, [arXiv:nucl-ex/0306021](#) [nucl-ex].
91. CMS, V. Khachatryan et al., *Charged-particle nuclear modification factors in PbPb and pPb collisions at $\sqrt{s_{NN}} = 5.02$ TeV*, JHEP **04** (2017) 039, [arXiv:1611.01664](#) [nucl-ex].
 92. X. Zhang and J. Liao, *Jet Quenching and Its Azimuthal Anisotropy in AA and possibly High Multiplicity pA and dA Collisions*, [arXiv:1311.5463](#) [nucl-th].
 93. C. Park, C. Shen, S. Jeon, and C. Gale, *Rapidity-dependent jet energy loss in small systems with finite-size effects and running coupling*, [arXiv:1612.06754](#) [nucl-th].
 94. K. Tywoniuk, *Is there jet quenching in pPb?*, Nucl. Phys. **A926** (2014) 85–91.
 95. D. V. Perepelitsa, *Hard processes in small systems*, in *26th International Conference on Ultrarelativistic Nucleus-Nucleus Collisions (Quark Matter 2017) Chicago, Illinois, USA, February 6-11, 2017*. 2017. [arXiv:1707.03839](#) [nucl-ex].
<https://inspirehep.net/record/1609809/files/arXiv:1707.03839.pdf>.
 96. ALICE, J. Adam et al., *Centrality dependence of particle production in p-Pb collisions at $\sqrt{s_{NN}} = 5.02$ TeV*, Phys. Rev. **C91** (2015) no. 6, 064905, [arXiv:1412.6828](#) [nucl-ex].
 97. ALICE, J. Adam et al., *Centrality dependence of charged jet production in p-Pb collisions at $\sqrt{s_{NN}} = 5.02$ TeV*, Eur. Phys. J. **C76** (2016) no. 5, 271, [arXiv:1603.03402](#) [nucl-ex].
 98. ATLAS, G. Aad et al., *Measurement of long-range pseudorapidity correlations and azimuthal harmonics in $\sqrt{s_{NN}} = 5.02$ TeV proton-lead collisions with the ATLAS detector*, Phys. Rev. **C90** (2014) no. 4, 044906, [arXiv:1409.1792](#) [hep-ex].
 99. A. Adare et al., *An Upgrade Proposal from the PHENIX Collaboration*, [arXiv:1501.06197](#) [nucl-ex].
 100. M. L. Miller, K. Reygers, S. J. Sanders, and P. Steinberg, *Glauber modeling in high energy nuclear collisions*, Ann. Rev. Nucl. Part. Sci. **57** (2007) 205–243, [arXiv:nucl-ex/0701025](#) [nucl-ex].
 101. K. Welsh, J. Singer, and U. W. Heinz, *Initial state fluctuations in collisions between light and heavy ions*, Phys. Rev. **C94** (2016) no. 2, 024919, [arXiv:1605.09418](#) [nucl-th].
 102. W. Broniowski, M. Rybczynski, and P. Bozek, *GLISSANDO: Glauber initial-state simulation and more...*, Comput. Phys. Commun. **180** (2009) 69–83, [arXiv:0710.5731](#) [nucl-th].
 103. J. Noronha-Hostler, J. Noronha, and M. Gyulassy, *Sensitivity of flow harmonics to subnucleon scale fluctuations in heavy ion collisions*, Phys. Rev. **C93** (2016) no. 2, 024909, [arXiv:1508.02455](#) [nucl-th].
 104. F. Gelis and B. Schenke, *Initial State Quantum Fluctuations in the Little Bang*, Ann. Rev. Nucl. Part. Sci. **66** (2016) 73–94, [arXiv:1604.00335](#) [hep-ph].
 105. M. Habich, G. A. Miller, P. Romatschke, and W. Xiang, *Testing hydrodynamic descriptions of p+p collisions at $\sqrt{s} = 7$ TeV*, Eur. Phys. J. **C76** (2016) no. 7, 408, [arXiv:1512.05354](#) [nucl-th].
 106. S. Schlichting and B. Schenke, *The shape of the proton at high energies*, Phys. Lett. **B739** (2014) 313–319, [arXiv:1407.8458](#) [hep-ph].
 107. H. Mäntysaari, B. Schenke, C. Shen, and P. Tribedy, *Imprints of fluctuating proton shapes on flow in proton-lead collisions at the LHC*, Phys. Lett. **B772** (2017) 681–686, [arXiv:1705.03177](#) [nucl-th].
 108. K. Geiger and B. Muller, *Dynamics of parton cascades in highly relativistic nuclear collisions*, Nucl. Phys. **B369** (1992) 600–654.
 109. B. Zhang, *ZPC 1.0.1: A Parton cascade for ultrarelativistic heavy ion collisions*, Comput. Phys. Commun. **109** (1998) 193–206, [arXiv:nucl-th/9709009](#) [nucl-th].
 110. B. Zhang, M. Gyulassy, and C. M. Ko, *Elliptic flow from a parton cascade*, Phys. Lett. **B455**

- (1999) 45–48, [arXiv:nucl-th/9902016](#) [nucl-th].
111. D. Molnar and M. Gyulassy, *New solutions to covariant nonequilibrium dynamics*, Phys. Rev. **C62** (2000) 054907, [arXiv:nucl-th/0005051](#) [nucl-th].
 112. D. Molnar and M. Gyulassy, *Saturation of elliptic flow and the transport opacity of the gluon plasma at RHIC*, Nucl. Phys. **A697** (2002) 495–520, [arXiv:nucl-th/0104073](#) [nucl-th]. [Erratum: Nucl. Phys.A703,893(2002)].
 113. D. Molnar and S. A. Voloshin, *Elliptic flow at large transverse momenta from quark coalescence*, Phys. Rev. Lett. **91** (2003) 092301, [arXiv:nucl-th/0302014](#) [nucl-th].
 114. Z. Xu and C. Greiner, *Thermalization of gluons in ultrarelativistic heavy ion collisions by including three-body interactions in a parton cascade*, Phys. Rev. **C71** (2005) 064901, [arXiv:hep-ph/0406278](#) [hep-ph].
 115. Z.-W. Lin, C. M. Ko, B.-A. Li, B. Zhang, and S. Pal, *A Multi-phase transport model for relativistic heavy ion collisions*, Phys. Rev. **C72** (2005) 064901, [arXiv:nucl-th/0411110](#) [nucl-th].
 116. Z. Xu and C. Greiner, *Shear viscosity in a gluon gas*, Phys. Rev. Lett. **100** (2008) 172301, [arXiv:0710.5719](#) [nucl-th].
 117. L. He, T. Edmonds, Z.-W. Lin, F. Liu, D. Molnar, and F. Wang, *Anisotropic parton escape is the dominant source of azimuthal anisotropy in transport models*, Phys. Lett. **B753** (2016) 506–510, [arXiv:1502.05572](#) [nucl-th].
 118. A. Bzdak and G.-L. Ma, *Elliptic and triangular flow in p+Pb and peripheral Pb+Pb collisions from parton scatterings*, Phys. Rev. Lett. **113** (2014) no. 25, 252301, [arXiv:1406.2804](#) [hep-ph].
 119. J. D. Orjuela Koop, A. Adare, D. McGlinchey, and J. L. Nagle, *Azimuthal anisotropy relative to the participant plane from a multiphase transport model in central p + Au , d + Au , and $^3\text{He} + \text{Au}$ collisions at $\sqrt{s_{NN}} = 200$ GeV*, Phys. Rev. **C92** (2015) no. 5, 054903, [arXiv:1501.06880](#) [nucl-ex].
 120. H. Li, L. He, Z.-W. Lin, D. Molnar, F. Wang, and W. Xie, *Origin of the mass splitting of azimuthal anisotropies in a multiphase transport model*, Phys. Rev. **C96** (2017) no. 1, 014901, [arXiv:1604.07387](#) [nucl-th].
 121. L. Yan, S. Pal, and J.-Y. Ollitrault, *Nonlinear hydrodynamic response confronts LHC data*, Nucl. Phys. **A956** (2016) 340–343, [arXiv:1601.00040](#) [nucl-th].
 122. P. Danielewicz and M. Gyulassy, *Dissipative Phenomena in Quark Gluon Plasmas*, Phys. Rev. **D31** (1985) 53–62.
 123. K. Dusling, W. Li, and B. Schenke, *Novel collective phenomena in high-energy proton–proton and proton–nucleus collisions*, Int. J. Mod. Phys. **E25** (2016) no. 01, 1630002, [arXiv:1509.07939](#) [nucl-ex].
 124. K. Dusling and R. Venugopalan, *Azimuthal collimation of long range rapidity correlations by strong color fields in high multiplicity hadron-hadron collisions*, Phys. Rev. Lett. **108** (2012) 262001, [arXiv:1201.2658](#) [hep-ph].
 125. A. Dumitru, K. Dusling, F. Gelis, J. Jalilian-Marian, T. Lappi, and R. Venugopalan, *The Ridge in proton-proton collisions at the LHC*, Phys. Lett. **B697** (2011) 21–25, [arXiv:1009.5295](#) [hep-ph].
 126. B. Schenke, *Origins of collectivity in small systems*, in *26th International Conference on Ultrarelativistic Nucleus-Nucleus Collisions (Quark Matter 2017) Chicago, Illinois, USA, February 6-11, 2017*. 2017. [arXiv:1704.03914](#) [nucl-th]. <https://inspirehep.net/record/1591565/files/arXiv:1704.03914.pdf>.
 127. A. Ortiz Velasquez, P. Christiansen, E. Cuautle Flores, I. Maldonado Cervantes, and G. Paić, *Color Reconnection and Flowlike Patterns in pp Collisions*, Phys. Rev. Lett. **111** (2013) no. 4,

- 042001, [arXiv:1303.6326](#) [hep-ph].
128. M. Gyulassy, P. Levai, I. Vitev, and T. S. Biro, *Non-Abelian Bremsstrahlung and Azimuthal Asymmetries in High Energy $p + A$ Reactions*, Phys. Rev. **D90** (2014) no. 5, 054025, [arXiv:1405.7825](#) [hep-ph].
 129. A. Kovner and M. Lublinsky, *Angular Correlations in Gluon Production at High Energy*, Phys. Rev. **D83** (2011) 034017, [arXiv:1012.3398](#) [hep-ph].
 130. B. Blok, C. D. Jäkel, M. Strikman, and U. A. Wiedemann, *Collectivity from interference*, [arXiv:1708.08241](#) [hep-ph].
 131. E. Iancu and A. H. Rezaeian, *Elliptic flow from color-dipole orientation in pp and pA collisions*, Phys. Rev. **D95** (2017) no. 9, 094003, [arXiv:1702.03943](#) [hep-ph].
 132. M. Greif, C. Greiner, B. Schenke, S. Schlichting, and Z. Xu, *Importance of initial and final state effects for azimuthal correlations in $p+Pb$ collisions*, [arXiv:1708.02076](#) [hep-ph].
 133. I. Muller, *Zum Paradoxon der Wärmeleitungstheorie*, Z. Phys. **198** (1967) 329–344.
 134. W. Israel, *Nonstationary irreversible thermodynamics: A Causal relativistic theory*, Annals Phys. **100** (1976) 310–331.
 135. W. Israel and J. M. Stewart, *Transient relativistic thermodynamics and kinetic theory*, Annals Phys. **118** (1979) 341–372.
 136. M. Spaliński, *Small systems and regulator dependence in relativistic hydrodynamics*, Phys. Rev. **D94** (2016) no. 8, 085002, [arXiv:1607.06381](#) [nucl-th].
 137. R. Baier, P. Romatschke, D. T. Son, A. O. Starinets, and M. A. Stephanov, *Relativistic viscous hydrodynamics, conformal invariance, and holography*, JHEP **04** (2008) 100, [arXiv:0712.2451](#) [hep-th].
 138. G. S. Denicol, J. Noronha, H. Niemi, and D. H. Rischke, *Origin of the Relaxation Time in Dissipative Fluid Dynamics*, Phys. Rev. **D83** (2011) 074019, [arXiv:1102.4780](#) [hep-th].
 139. G. S. Denicol, H. Niemi, E. Molnar, and D. H. Rischke, *Derivation of transient relativistic fluid dynamics from the Boltzmann equation*, Phys. Rev. **D85** (2012) 114047, [arXiv:1202.4551](#) [nucl-th]. [Erratum: Phys. Rev.D91,no.3,039902(2015)].
 140. S. Bhattacharyya, V. E. Hubeny, S. Minwalla, and M. Rangamani, *Nonlinear Fluid Dynamics from Gravity*, JHEP **02** (2008) 045, [arXiv:0712.2456](#) [hep-th].
 141. P. Romatschke, *Relativistic Viscous Fluid Dynamics and Non-Equilibrium Entropy*, Class. Quant. Grav. **27** (2010) 025006, [arXiv:0906.4787](#) [hep-th].
 142. Y. Bu and M. Lublinsky, *All order linearized hydrodynamics from fluid-gravity correspondence*, Phys. Rev. **D90** (2014) no. 8, 086003, [arXiv:1406.7222](#) [hep-th].
 143. S. Grozdanov and N. Kaplis, *Constructing higher-order hydrodynamics: The third order*, Phys. Rev. **D93** (2016) no. 6, 066012, [arXiv:1507.02461](#) [hep-th].
 144. P. Romatschke and U. Romatschke, *Relativistic Fluid Dynamics Out of Equilibrium – Ten Years of Progress in Theory and Numerical Simulations of Nuclear Collisions*, [arXiv:1712.05815](#) [nucl-th].
 145. M. P. Heller, R. A. Janik, and P. Witaszczyk, *Hydrodynamic Gradient Expansion in Gauge Theory Plasmas*, Phys. Rev. Lett. **110** (2013) no. 21, 211602, [arXiv:1302.0697](#) [hep-th].
 146. A. Buchel, M. P. Heller, and J. Noronha, *Entropy Production, Hydrodynamics, and Resurgence in the Primordial Quark-Gluon Plasma from Holography*, Phys. Rev. **D94** (2016) no. 10, 106011, [arXiv:1603.05344](#) [hep-th].
 147. M. P. Heller and M. Spalinski, *Hydrodynamics Beyond the Gradient Expansion: Resurgence and Resummation*, Phys. Rev. Lett. **115** (2015) no. 7, 072501, [arXiv:1503.07514](#) [hep-th].

148. M. P. Heller, R. A. Janik, and P. Witaszczyk, *The characteristics of thermalization of boost-invariant plasma from holography*, Phys. Rev. Lett. **108** (2012) 201602, [arXiv:1103.3452 \[hep-th\]](#).
149. V. Baranov and M. Ruderman, *On the effect of transport coefficient anisotropy on the plasma flow in heliospheric interface*, Monthly Notices of the Royal Astronomical Society **434** (2013) no. 4, 3202–3207.
150. J. Casalderrey-Solana, M. P. Heller, D. Mateos, and W. van der Schee, *From full stopping to transparency in a holographic model of heavy ion collisions*, Phys. Rev. Lett. **111** (2013) 181601, [arXiv:1305.4919 \[hep-th\]](#).
151. P. M. Chesler, M. Lekaveckas, and K. Rajagopal, *Heavy quark energy loss far from equilibrium in a strongly coupled collision*, JHEP **10** (2013) 013, [arXiv:1306.0564 \[hep-ph\]](#).
152. W. van der Schee, *Early hydrodynamisation, energy loss and small systems in holographic heavy ion collisions*, EPJ Web Conf. **137** (2017) 07023.
153. E. Shuryak and I. Zahed, *High-multiplicity pp and pA collisions: Hydrodynamics at its edge*, Phys. Rev. **C88** (2013) no. 4, 044915, [arXiv:1301.4470 \[hep-ph\]](#).
154. G. Başar and D. Teaney, *Scaling relation between pA and AA collisions*, Phys. Rev. **C90** (2014) no. 5, 054903, [arXiv:1312.6770 \[nucl-th\]](#).
155. P. M. Chesler, *Colliding shock waves and hydrodynamics in small systems*, Phys. Rev. Lett. **115** (2015) no. 24, 241602, [arXiv:1506.02209 \[hep-th\]](#).
156. P. M. Chesler, *How big are the smallest drops of quark-gluon plasma?*, JHEP **03** (2016) 146, [arXiv:1601.01583 \[hep-th\]](#).